TITLE

A novel system to map protein interactions reveals evolutionarily conserved immune evasion pathways on transmissible cancers

SHORT TITLE

Immune checkpoints on transmissible cancers

AUTHORS

Andrew S. Flies[1]*, Jocelyn M. Darby[1], Patrick R. Lennard[1,2], Peter R. Murphy[1,3], Chrissie E. B. Ong[1], Terry L. Pinfold[4], A. Bruce Lyons[4], Gregory M. Woods[1], Amanda L. Patchett[1]

AFFILIATIONS

[1]Menzies Institute for Medical Research, College of Health and Medicine, University of Tasmania, Hobart, TAS 7000, Australia

[2]The Roslin Institute and Royal School of Veterinary Studies, University of Edinburgh, Easter Bush Campus, Midlothian, EH25 9RG, UK

[3]University of Queensland Diamantina Institute, The University of Queensland, Translational Research Institute, Woolloongabba, Queensland, Australia

[4]School of Medicine, College of Health and Medicine, University of Tasmania, Hobart, TAS 7000, Australia

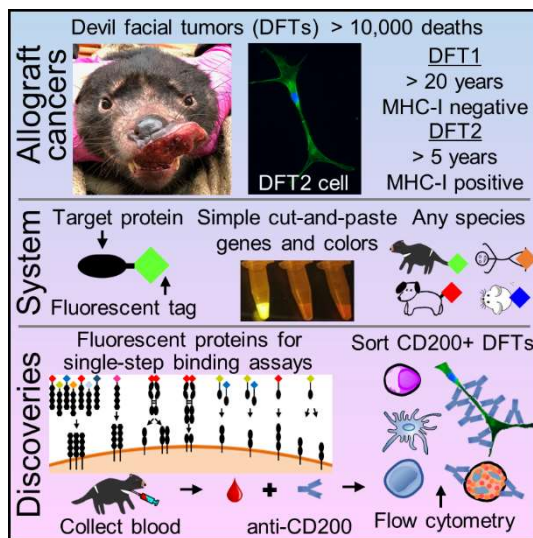**CORRESPONDING AUTHOR CONTACT INFORMATION**

23   **Andrew S. Flies, PhD**

24   Menzies Institute for Medical Research, College of Health and Medicine

25   University of Tasmania

26   Private Bag 23, Hobart TAS 7000

27   phone: +61 3 6226 4614; email: Andy.Flies@utas.edu.au

28

29   **GRAPHICAL ABSTRACT**

30

31

32

ABSTRACT

Immune checkpoint immunotherapy has revolutionized medicine, but translational success for new treatments remains low. Around 40% of humans and Tasmanian devils (*Sarcophilus harrisii*) develop cancer in their lifetime, compared to less than 10% for most species. Additionally, devils are affected by two of the three known transmissible cancers in mammals. Unfortunately, little is known about of immune checkpoints in devils and other non-model species, largely due to a lack of species-specific reagents. We developed a simple cut-and-paste reagent development method applicable to any vertebrate species and show that immune checkpoint interactions are conserved across 160 million years of evolution. The inhibitory checkpoint molecule CD200 is highly expressed on devil facial tumor cells. We are the first to demonstrate that co-expression of CD200R1 can block CD200 expression. The evolutionarily conserved pathways suggest that naturally occurring cancers in devils and other species can serve as models for understanding cancer and immunological tolerance.

KEYWORDS

immune checkpoint, wild immunology, reagent development, marsupial, transmissible cancer

INTRODUCTION

Metastatic cancer affects most mammals, but the cancer incidence can vary widely across phylogenetic groups and species (**Figure 1, Table S1**) [1–9]. In humans, the lifetime risk of developing cancer is around 40% [10]. This is in stark contrast to a general cancer incidence of 3% for mammals, 2% for birds, and 2% for reptiles reported by the San Diego Zoo (n=10,317) [7,11]. A more recent study at the Taipei Zoo reported cancer incidence of 8%, 4%, and 1% for mammals, birds, and reptiles, respectively (n=2,657) [4]. Cancer incidence in domestic animals is generally less than 10% (n=202,277) [9]. However, two studies performed 40 years apart reported that greater than 40% of Tasmanian devils develop spontaneous, often severe neoplasia in their lifetime [11,12]. Devils are also unique because they are affected by two of the three known naturally-occurring transmissible cancers in vertebrate species [13,14]. Transmissible cancers are a distinct form of cancer in which the tumor cells function as an infectious pathogen and an allograft. Dogs (*Canis lupus familiaris*) are the only other vertebrate species affected by a transmissible cancer [15], and interestingly some breeds of dogs also have high cancer incidence [9,16].

The devil facial tumor (DFT) disease was first detected in Northwest Tasmania and has been a primary driver of an 80% decline in the wild Tasmanian devil population [13,17]. The clonal devil facial tumor (DFT1) cells have been continually transmitted among devils and is estimated to have killed at least 10,000 individuals since at least 1996. In 2014 a second independent transmissible Tasmanian devil facial tumor (DFT2) was discovered in wild devils [14] and 23 cases have been reported to date [18]. Genetic mismatches, particularly in the major histocompatibility complex (MHC) genes should lead to rejection of these transmissible tumors. Consequently, the role of devil MHC has been a focus of numerous studies (**Figure 1, Table S1**) to understand the lack of rejection of the transmissible tumors. These studies have revealed that the DFT1 cells

74   downregulate MHC class I (MHC-I) expression [19], a phenomenon observed in many human

75   cancers [20]. In contrast to DFT1 cells, the DFT2 cells do express MHC-I [21]. DFT1 and DFT2 cells

76   also have 2,884 and 3,591 single nucleotide variants, respectively, that are not present in 46 normal

77   devil genomes [22]. The continual transmission of DFT1 and DFT2, despite MHC-I expression by

78   DFT2 cells and genetic mismatches between host and tumor, suggests that additional pathways are

79   likely involved in immune evasion.

80   Human cancer treatment has been revolutionized in the past decade by manipulating

81   interactions among immune checkpoint molecules [23,24]. These have proven broadly effective in

82   part because they function across many different MHC types and tumor mutational patterns.

83   However, these pathways have received little attention in transmissible cancers and other naturally

84   occurring cancers in non-model species (**Figure 1, Table S1**) [25–27]. We have previously shown that

85   the inhibitory immune checkpoint molecule programmed death ligand 1 (PDL1) is expressed in

86   the DFT microenvironment and is upregulated by interferon-gamma (IFNγ) *in vitro* [25]. This finding

87   led us to question which other immune checkpoint molecules play a role in immune evasion by

88   the transmissible cancers and the devil's high spontaneous cancer incidence. Understanding this

89   immune evasion in a natural environment has the potential to help protect this endangered species

90   and identify protein interactions that are conserved across divergent species to improve

91   translational success of animal models [27]. Unfortunately, a persistent limitation for immunology

92   in non-traditional study species is a lack of species-specific reagents. Wildlife biologists and

93   veterinarians are at the front lines of emerging infectious disease outbreaks, but they often lack

94   species-specific reagents to fulfil the World Health Organization's call for "cross-cutting R&D

95   preparedness" and perform mechanistic immunological investigations [28].

96   To solve the paucity of reagents available for Tasmanian devils and address ongoing

97 limitations for non-traditional study species, we developed a Fluorescent Adaptable Simple

98 Theranostic (FAST) protein system that builds upon the diverse uses of fluorescent proteins

99 previously reported [29–33]. This simple system can be used for rapid development of diagnostic and

100 therapeutic (i.e. theranostic) immunological toolkits for any animal species (**Figure 2**). We

101 demonstrate the versatility and impact of the FAST system by using it to confirm seven receptor-

102 ligand interactions among twelve checkpoint proteins in devils.

103   In humans, these checkpoint proteins have been targets of immunotherapy in clinical trials,

104 but the functional role and binding patterns of these proteins are unknown for most other species.

105 We have used the FAST system to show that the inhibitory checkpoint protein CD200 is highly

106 expressed on DFT cells, opening the door to single-cell phenotyping of circulating tumor cells

107 (CTCs) in devil blood. Furthermore, we are the first to report that co-expression of CD200R1 can

108 block surface expression of CD200 in any species. Understanding how clonal tumor cells graft

109 onto new hosts, evade immune defenses and metastasize within a host will identify evolutionarily

110 conserved immunological mechanisms to help improve cancer, infectious disease, and transplant

111 outcomes for human and veterinary medicine.

112

113 **RESULTS**

114 **Fluorescent fusion proteins can be secreted from mammalian cells**

115   Initially, we developed FAST proteins to determine whether monomeric fluorescent

116 proteins could be fused to devil proteins and secreted from mammalian cells (**Figure 2A** and **Table**

117 **S2**). We used 41BB (TNFRSF9) for proof-of-concept studies by fusing the extracellular domain

118 of devil 41BB checkpoint molecule to monomeric fluorescent proteins (**Figure 2A-B** and **Figure**

6

119   **S1**). We used wild-type Chinese hamster ovary (CHO) cells and CHO cells transfected with

120   41BBL (TNFSF9) to confirm specificity of the 41BB FAST proteins and demonstrate that the

121   fluorescent proteins (mAzurite, mCerulean3, mCherry, mCitrine, mOrange, Neptune2, and mTag-

122   BFP (aka mBFP)) remained fluorescent when secreted from mammalian cells (**Figure 2C**).

123   We chose mCherry, mCitrine, mOrange, and mBFP for ongoing FAST protein

124   development. Initial batches of FAST proteins were purified using the 6xHis-tag and eluted with

125   imidazole. The gradient of FAST protein in the collection tubes was apparent when excited with

126   blue light and visualized with an amber filter unit (**Figure 2D**), allowing immediate confirmation

127   that the fluorescent protein DNA coding sequences were in-frame and the proteins were properly

128   folded. mCherry was visible without excitation or filters (**Figure 2E**). After combining,

129   concentrating, and sterile filtering the eluted fractions, 100 μL was aliquoted and visualized again

130   using blue light to confirm fluorescent signal (**Figure 2F**). A full step-by-step protocol and set of

131   experimental templates for creating and testing FAST proteins for any species is available online

132   with the supplementary material.

133   **Receptor-ligand binding confirmed in single-step staining assays**

134   We chose additional immune checkpoint molecules for FAST protein development

135   (**Figure 3A**) based on targets of clinical trials and sequence analysis of devil genes [27,34,35]. We

136   transfected the FAST protein expression vectors (**Table S2**) into CHO cells and tested the

137   supernatant against CHO cell lines expressing full-length receptors. 41BB FAST proteins in

138   supernatant exhibited strong binding to 41BBL cell lines, but the fluorescent signals from most

139   other FAST proteins were too weak to confirm binding to the expected receptors (**Figure S2**). As

140   FAST proteins do not require secondary reagents, we next incubated target cells with purified

141   FAST proteins and added chloroquine to block the lysosomal protein degradation pathway [36]. This

142 allowed us to take advantage of receptor-mediated endocytosis, which can allow accumulation of

143 captured fluorescent signals inside the target cells [37]. This protocol adjustment allowed

144 confirmation that CD47-mCherry, CD200-mBFP, CD200-mOrange, CD200R1-mBFP, and

145 CD200R1-mOrange, and PD1-mCitrine bound to their expected receptors (**Figure 3B**). We also

146 demonstrated the flexibility of the FAST proteins by showing that alternative fusion conformations

147 (**Figure S1C-D**), such as type II proteins (e.g. mCherry-41BBL) and a devil Fc-tag (e.g. CD80-

148 Fc-mCherry) bound to their expected ligands (**Figure 3B**). The stability of the fusion proteins was

149 demonstrated using supernatants that were stored at 4 °C for two months prior to use in a one-hour

150 live-culture assay with chloroquine (**Figure S3**).

151 **Cell lines secreting FAST proteins confirm protein interactions in live coculture assays**

152   To further streamline the reagent development process, we next took advantage of the

153 single-step nature of FAST proteins (i.e. no secondary antibodies or labels needed) in live-cell

154 coculture assays (**Figure 4A**). Cell lines secreting 41BB-mCherry, 41BBL-mCherry, or CD80-Fc-

155 mCherry FAST proteins were mixed with cell lines expressing full-length 41BB, 41BBL, or

156 CTLA4-mCitrine and cocultured at a 1:1 ratio overnight with chloroquine. Singlet cells were gated

157 (**Figure 4B**) and binding of mCherry FAST proteins to CFSE or mCitrine-labelled target cells was

158 analyzed (**Figure 4C**). The strongest fluorescent signal from 41BB-mCherry, 41BBL-mCherry

159 and CD80-Fc-mCherry were detected when cocultured with their predicted receptors, 41BBL,

160 41BB and CTLA4, respectively.

161 **Optimization of the FAST-Fc construct**

162   The fluorescent binding signal of CD80-Fc-mCherry was lower than expected, so we next

163 re-examined our Fc-tag construct. In humans and all other mammals examined to date the IgG

164 heavy chain has glycine-lysine (Gly-Lys) residues at the C-terminus [38]; the initial devil IgG

8

165 constant region sequence available to us had an incomplete C-terminus, and thus our initial CD80-

166 Fc-mCherry vector did not have the C-terminal Gly-Lys. We subsequently made a new FAST-Fc

167 construct with CTLA4-Fc-mCherry, which exhibited strong binding to both CD80 and CD86

168 transfected DFT cells (**Figure 4D**).

169 **CD200 mRNA and protein are highly expressed in DFT cells**

170   Analysis of previously published devil and DFT cell transcriptomes suggested that CD200

171 mRNA is highly expressed in DFT2 cells and peripheral nerves, moderately expressed in DFT1

172 cells, and lower in other healthy devil tissues (**Figure 5A**) [34,35,39]. As CD200 is an inhibitory

173 molecule expressed on most human neuroendocrine neoplasms [40], and both DFT1 and DFT2

174 originated from Schwann cells [35,41], we sought to investigate CD200 expression on DFT cells at

175 the protein level. Staining of wild-type DFT1 and DFT2 cells with CD200R1-mOrange FAST

176 protein showed minimal fluorescent signal (**Figure 5B**). However, overexpression of CD200 using

177 a human EF1α promoter yielded a detectable signal with CD200R1-mOrange binding to CD200

178 on DFT1 cells. A weak signal from CD200-mOrange was detected on DFT1 cells overexpressing

179 CD200R1 (**Figure 5B**). To confirm naturally-expressed CD200 on DFT cells we digested CD200

180 and 41BB FAST proteins using TEV protease to remove the linker and fluorescent reporter. The

181 digested proteins were then used to immunize mice for polyclonal sera production. We stained

182 target CHO cell lines with pre-immune (PI) or immune (I) mouse sera collected after 3X

183 immunizations. Only the immune sera showed strong binding to the respective CD200 and 41BB

184 target cell lines (**Figure 5C**). After the final immunization (4X), we collected another batch of sera

185 and tested it on DFT1 and DFT2 cells (**Figure 5D**). In agreement with the transcriptomic data for

186 DFT cells [34], the polyclonal sera revealed high levels of CD200 on DFT cells, but low levels of

187 41BB.

Overexpression of CD200R1 blocks surface expression of CD200

In humans, overexpression of some checkpoint proteins can block surface expression of heterophilic binding partners in *cis* (e.g. CD80 and PDL1) [42,43]. As a potential route for disrupting the inhibitory effects of CD200 on anti-tumor immunity, we tested if overexpression of CD200R1 on DFT cells could reduce CD200 surface expression. We stained a DFT1 strain C5065, and DFT1 C5065 cells transfected to overexpress CD200 or CD200R1 with polyclonal anti-CD200 sera and secondary anti-mouse IgG AF647. We detected no surface protein expression of CD200 DFT1 cells overexpressing CD200R1 (**Figure 5E**).

Identification of DFT cells in whole blood using anti-CD200

In addition to high expression of CD200 on neuroendocrine neoplasms [40,44], CD200 is used as a diagnostic marker for several human blood cancers [45–47]. DFT cells metastasize in the majority of cases [48] and our transcriptome results (**Figure 5A**) suggest that CD200 mRNA is more highly expressed in DFT cells than in peripheral blood mononuclear cells (PBMCs) [34,35]. As a result, we tested if CD200 could be used to identify DFT cells in blood. We stained PBMCs and DFT2 cells separately with polyclonal anti-CD200 sera and anti-mouse AlexaFluor 647 and then analyzed CD200 expression by flow cytometry (**Figure S4A**). We then mixed the stained PBMCs and DFT2 cells at ratios of 1:10 (**Figure S4A**) and 1:5 (**Figure S4B**) and analyzed the mixed populations. PBMCs showed minimal CD200 expression and background staining (**Figure S4**), whereas CD200 was highly expressed on DFT2 cells. CD200+ DFT2 cells were readily distinguishable from PBMCs.

As our RNAseq results only included mononuclear cells, we next performed a pilot test to determine if DFT cells could be spiked into whole devil blood and identified via flow cytometry using CD200 staining. DFT1 and DFT2 cells were labeled with CellTrace violet (CTV) and 10,000

10

211   cells were diluted directly into 100 μL of whole blood from a healthy devil (n=1/treatment; n = 1

212   devil). The cells were then stained with purified polyclonal anti-CD200 with and without

213   secondary anti-mouse IgG AF647 prior to red blood cell (RBC) lysis. Initial results showed that

214   DFT2 cells expressed CD200 above the leukocyte background, but that DFT1 cells could not be

215   distinguished from leukocytes (**Figure S5**). To eliminate the secondary antibody step from the

216   whole blood staining protocol we next labelled the polyclonal anti-CD200 and normal mouse

217   serum (NMS) with a no-wash Zenon mouse IgG AF647 labeling reagent (n = 1/treatment; n = 2

218   devils). This system again showed that CD200 expression could be used to identify DFT2 cells in

219   blood (**Figure 6**), suggesting that CD200 is a candidate marker for identification of metastasizing

220   DFT2 cells.

221

222   **DISCUSSION**

223   Naturally occurring cancers provide a unique opportunity to study immune evasion and the

224   metastatic process across diverse hosts and environments. The exceptionally high cancer rate in

225   Tasmanian devils coupled with the two transmissible tumors currently circulating in the wild

226   warrants a thorough investigation of the devil immune system. However, taking advantage of such

227   natural disease models has been out of reach for most species due to a lack of reagents. The FAST

228   protein system we developed here is well-suited to discovering additional DFT markers, and more

229   generally, filling the reagent gap for non-traditional species. For proteins like 41BB that have high

230   affinity for 41BBL, FAST proteins can be used as detection reagents directly from supernatant.

231   For other molecules with lower receptor-ligand affinity, the FAST proteins can be purified,

232   digested with a protease to remove the non-target proteins and used for production of polyclonal

233   or monoclonal antibodies.

11

234 The simple cut-and-paste methods for vector assembly lend the FAST protein system to

235 entry level immunology and molecular biology skill sets. Additionally, the ability of FAST

236 proteins to be used in live coculture assays and with elimination of secondary reagents, will

237 increase efficiency and reduce experimental error for advanced human and mouse cancer

238 immunology studies. For example, previous high-throughput studies have used a two-step staining

239 process (i.e. recombinant protein + secondary antibody) to screen more than 2000 protein

240 interactions [49,50]; this type of assay can be streamlined using FAST proteins to eliminate the need

241 for secondary antibodies. Fc-tags or other homodimerization domains can be incorporated into

242 FAST proteins to increase binding for low-affinity interactions.

243 Production of recombinant proteins in cell lines that closely resemble the physiological

244 conditions of the native cell type (i.e. mammalian proteins produced in mammalian cell lines) are

245 more likely to yield correct protein folding, glycosylation, and function than proteins produced

246 using evolutionarily distant cell lines [51]. The fluorescent fusion proteins developed here that take

247 advantage of natural receptor expression and cycling processes (e.g. CTLA4 transendocytosis) in

248 eukaryotic target cells; bacterial protein production methods are not amenable to coculture with

249 eukaryotic target cells in immunological assays [52]. Our demonstration of the FAST protein system

250 in CHO cells, which are used to produce approximately 70% of recombinant pharmaceutical

251 proteins [53], suggest that this method can be efficiently integrated into existing research and

252 development pipelines for humans and other vertebrate species.

253 A primary question in transmissible tumor research is why genetically mismatched cells

254 are not rejected by the host. Successful infection of devils with DFT cells relies on the ability of

255 the tumor allograft to evade and manipulate host defences. The "missing-self" hypothesis suggests

256 that the lack of constitutive MHC-I expression on DFT1 cells should lead to natural killer (NK)

257   cell-mediated killing of the allograft tumor cells. Here we used the FAST protein system to develop

258   a tool set to address this question and show that DFT1 and DFT2 cells express CD200 at higher

259   levels than most other devil tissues examined to date. CD200 has been shown to directly inhibit

260   NK cells in other species [54–56], so overexpression of CD200 is a potential mechanism of immune

261   evasion of NK responses by DFT cells.

262   We hypothesize that CD200 could be particularly important in DFT transmission as the

263   CD200-CD200R pathway is critical to the initial stages of establishing transplant and allograft

264   tolerance in other species [57–59]. In line with this hypothesis, a recent study reported that

265   overexpressing several checkpoint molecules, including CD200, PDL1, and CD47, in mouse

266   embryonic stem cells could be used to generate teratomas that could establish long-term allograft

267   tolerance in fully immunocompetent hosts [60]. We have previously reported that PDL1 mRNA and

268   protein are upregulated on DFT2 cells in response to IFNγ [25], and our transcriptome results show

269   that CD47 is expressed at moderate to high levels in DFT cells. Here we show that overexpression

270   of CD200R1 on DFT1 eliminates binding of our polyclonal anti-CD200 antibodies, suggesting

271   that DFT cells overexpressing CD200R1 could be used to test the role of CD200 in allograft

272   tolerance. Alternatively, genetic ablation of CD200 in DFT cells could be used as a complementary

273   approach to examine the role of immune checkpoint molecules in DFT allograft tolerance. The

274   CD200-CD200R1 pathway has been implicated in reducing IFNγ production by dendritic cells [59]

275   and decreasing the responsiveness of myeloid cells to IFNγ stimulation [61]. Low MHC-I expression

276   is a primary means of immune evasion by DFT1 cells, and disrupting the CD200-CD200R1

277   pathway could facilitate improved recognition of DFT1 cells by CD8 T cells by enhancing IFNγ-

278   mediated MHC-I upregulation. Recent work in mice has identified immunosuppressive natural

279   regulatory plasma cells that express CD200, LAG3, PDL1, and PDL2; we have previously

280   identified PDL1+ cells with plasma cell morphology near or within the DFT microenvironment [25].

281   Previous DFT vaccine efforts have used killed DFT cells with adjuvants [62,63]. A similar

282   approach to treat gliomas in dogs reported that tumor-lysate with CD200 peptides nearly doubled

283   progression-free survival compared to tumor lysate alone [64]. Like devils, several breeds of dog are

284   prone to cancer and these genetically-outbred large animal models provide a fertile ground for

285   testing cancer therapies. Interestingly, the CD200 peptides are reported to provide agonistic

286   function through CD200-like activation receptors (CD200R4) rather than by blocking CD200R1

287   [44,64]. The functional role of CD200-CD200R pathway in devils remains to be elucidated, but the

288   CD200R1$_{NPLY}$ inhibitory motif and key tyrosine residues are conserved in devil CD200R [27,65,66],

289   demonstrating this motif is conserved over 160 million years of evolutionary history [67]. In addition

290   to agonistic peptides, several other options for countering CD200-CD200R immune inhibition are

291   possible. Human chronic lymphocytic leukemia cells often express high levels of CD200, which

292   can be downregulated in response to imiquimod [68]. Likewise, we have previously shown that DFT1

293   cells downregulate expression of CD200 mRNA *in vitro* in response to imiquimod treatment [34].

294   In mice, chronic salmonella and schistosoma infections upregulated both CD200 and

295   CD200R [69]. Several viruses, including cytomegalovirus [70] and herpesvirus [71] manipulated the

296   CD200-CD200R pathway as a means of immune evasion. Interestingly, in one of the longest

297   running and most in-depth studies of host-pathogen coevolution, CD200R was shown to be under

298   selection in rabbits in response to myxoma virus biocontrol agent [72]. As DFT1 and DFT2 have

299   been circulating in devils for more than 20 years and 5 years, respectively, it will be important to

300   monitor CD200/R expression and the potential evolution of paired activating and inhibitory

301   receptors in these natural disease models [73].

302   Immunophenotyping and single-cell RNAseq of circulating tumor cells (CTCs) has

303   potential to identify key gene expression patterns associated with metastasis and tissue invasion.

304   Periaxin (PRX) is the most sensitive and specific marker for DFT1 cells in immunohistochemistry

305   assays [74]. Unfortunately, PRX is expressed primarily in the cytoplasm, which eliminates the

306   possibility of using PRX as a marker to sort live cells via flow cytometry for single-cell RNAseq.

307   However, CD200 is a potential marker for the identification of circulating tumor cells (CTCs) from

308   devil blood. As proof of concept, DFT2 cells could be identified in devil blood spiked with DFT2

309   cells. As CTCs are likely to be rare in the blood of most infected devils, CD200 alone would be

310   insufficient for identifying DFT1 cells. Additional surface DFT markers would be required to

311   purify CTCs for metastases and tissue invasion analyses. The FAST protein system provides a

312   simple procedure to facilitate the production of a panel of DFT-markers to help identify key

313   proteins in the metastatic process.

314   In summary, the simple "cut-and-paste" production of the vectors and single-step testing

315   pipeline of the FAST system provided multiple benefits. The FAST system allowed us to

316   characterize receptor-ligand interactions, and to identify evolutionarily conserved immune evasion

317   pathways in naturally occurring transmissible cancers. Our initial implementation of the system

318   confirmed numerous predicted protein interactions for the first time in a marsupial species and

319   documented high expression of the inhibitory molecule CD200 on DFT cells. The high expression

320   of CD200 in devil nervous tissues and neuroendocrine tumors, downregulation of CD200 in

321   response to imiquimod, and binding of CD200 to CD200R1, is consistent with results from human

322   and mouse studies. Consequently, the CD200/R pathway provides a promising immunotherapy

323   and vaccine target for DFTs. Beyond this study, FAST proteins meet the key attributes needed for

324   reagent development, such as being straightforward to make, stable, versatile, renewable, cheap,

15

325 and amenable to high-throughput testing [75]. The direct fusion of the reporter protein to the protein-

326 of-interest allows for immediate feedback during transfection, supernatant testing, and protein

327 purification; proteins with frameshifts, introduced stop codons, or folded improperly will not

328 fluoresce and can be discarded after a simple visualization, rather than only after extensive

329 downstream testing. Efficient mapping of immune checkpoint interactions across species can

330 identify evolutionarily conserved immune evasion pathways and appropriate large animal models

331 with naturally occurring cancer. This knowledge could inform veterinary and human medicine in

332 the fields of immunological tolerance to tissue transplants, infectious disease, and cancer.

333

334 **MATERIALS AND METHODS**

335 **Study design**

336   The objectives of this study were to fill a major gap in our understanding of the mammalian

337 immune system and to understand how genetically mismatched transmissible tumors evade host

338 immunity. To achieve this goal, we developed a recombinant protein system that directly fuses

339 proteins-of-interest to a fluorescent reporter protein. The first phase was to determine if the

340 fluorescent protein remained fluorescent after secretion from mammalian cells and to confirm that

341 proteins bound to their predicted receptors (i.e. ligands). Initial testing was performed in CHO

342 cells and follow-up assays used devil cells. To further demonstrate the functionality of this system

343 for antibody development, mice were immunized with either 41BB or CD200 proteins. Pre- and

344 post-immunization polyclonal sera was used to confirm that the proteins used for immunization

345 induced antibodies that specifically bound to surface-expressed recombinant proteins and native

346 proteins on devil facial tumor cells.

347 **Target transcript amplification**

16

348   Target gene DNA sequences for vector construction were retrieved from Genbank,

349 Ensembl or de novo transcriptome assemblies (**Table S2**) [76]. Target DNA was amplified from a

350 cDNA template or existing plasmids using primers and PCR conditions shown in **Tables S2-S4**

351 using Q5 High-Fidelity 2X Master Mix (New England Biolabs # M0494L). Primers were ordered

352 with 5' base extensions that overlapped expression vectors on either side of the restriction sites.

353 The amplified products were identified by gel electrophesis and purified using Nucleospin PCR

354 and Gel Clean Up Kit (Macherey-Nagel # 740609.5). Alternatively, DNA sequences were

355 purchased as double stranded DNA gblocks (**Table S5**) (Integrated DNA Technologies) for direct

356 assembly into expression vectors.

357 **Construction of all-in-one Sleeping Beauty transposon vectors**

358   All new plasmids were assembled using NEBuilder kit (NEB # E5520S) following the

359 manufacturer's recommendations unless otherwise noted. DNA inserts, digested plasmids, and

360 NEBuilder master mix were incubated for 60 minutes at 50 °C and then transformed into DH5α

361 included with the NEBuilder kit. Plasmid digestions were performed following manufacturer

362 recommendations and generally subjected to Antarctic phosphatase (New England Biolabs #

363 M0289S) treatment to prevent potential re-annealing. Sleeping Beauty transposon vectors pSBbi-

364 Hyg (Addgene # 60524), pSBbi-BH (Addgene # 60515), pSBtet-Hyg (Addgene # 60508), pSBtet-

365 RH (Addgene # 60500) were gifts to Addgene from Eric Kowarz [77]. The pCMV(CAT)T7-SB100

366 containing the CMV promoter and SB100X transposase was a gift to Addgene from Zsuzsanna

367 Izsvak (Addgene # 34879) [78]. We first constructed an all-in-one Sleeping Beauty vector by

368 inserting a CMV promoter and SB100X transposase from pCMV(CAT)T7-SB100 [78] into pSBi-

369 BH [77] (**Tables S3-S4**). This was accomplished by using pAF111-vec.FOR and pAF111.1.REV

370 primers to amplify an overlap region from pSBbi-BH (insert 1) and pAF111-2.FOR and pAF111-

17

371   2.REV to amplify the CMV-SB100X region from pCMV(CAT)T7-SB100 (insert 2). The purified

372   amplicons were then used for NEBuilder assembly of pAF111. The final all-in-one vectors

373   pAF112 (hygromycin resistance and luciferase) and pAF123 (hygromycin resistance) were

374   assembled from the pAF111 components. pAF112 was assembled by amplifying the Luc2

375   luciferase gene (insert 1) from pSBtet-Hyg and the P2A-hygromycin resistance gene (insert 2)

376   from pSBbi-BH and inserting into the pAF111 Bsu36I digest using NEBuilder. pSBbi-Hyg was

377   Bsu36I-digested to obtain the hygromycin resistance gene, and this fragment was inserted into

378   Bsu36I-digested pAF111 using T4 ligase cloning to replace the BFP-P2A-hygromycin segment in

379   pAF111.

Construction of full-length protein vectors

381   All full-length gene coding sequences except CTLA4 were cloned into the a pAF112 SfiI

382   digest (**Table S2**). All full-length vectors also contain luciferase with T2A peptide linked to the

383   hygromycin resistance protein; luciferase was included for use in downstream functional testing

384   that was not part of this study. Tasmanian devil CTLA4 was cloned into a NotI-HF and XmaI

385   digest of pAF100 that was used in a different study but is derived from vectors pAF112 and

386   pAF138. Additionally, we also used devil PDL1 (CHO.pAF48) and 41BBL (CHO.pAF56) cell

387   lines developed using a vector system described previously [25].

Construction of FAST protein vectors

389   Plasmids containing fluorescent protein coding sequences mCerulean3-N1 (Addgene #

390   54730), mAzurite-N1 (Addgene # 54617), mOrange-N1 (Addgene # 54499), mNeptune2-N1

391   (Addgene # 54837) were gifts to Addgene from Michael Davidson. mTag-BFP was amplified from

392   pSBbi-BH, mCitrine was amplified from pAF71, and mCherry was amplified from pTRE-Dual2

393   (Clontech # PT5038-5). pAF137 was constructed by amplifying the devil 41BB extracellular

394   domain with primers pAF137-1.FOR and pAF137-1.REV and amplifying mCherry with pAF137-

395   2a.FOR and pAF137-2.REV (**Table S3-4**). 5' extensions on pAF137-1.FOR and pAF137-2.REV

396   were used to create overlaps for NEBuilder assembly of pAF137 from a pAF123 SfiI-digested

397   base vector. 3' extensions on pAF137-1.REV and pAF137-2a.FOR were used to create the linker

398   that included an XmaI/SmaI restriction site, TEV cleavage tag, GSAGSAAGSGEF linker peptide,

399   and 6x-His tag between the gene-of-interest and fluorescent reporter. The GSAGSAAGSGEF was

400   chosen due to the low number of large hydrophobic residues and less repeated nucleic acids than

401   are needed with other flexible linkers such as $(GGGS)_4$ [79]. The pAF137 primer extensions also

402   created 5' NotI and 3' NheI sites in the FAST vector to facilitate downstream swapping of

403   functional genes and to create a Kozak sequence [80] (GCCGCCACC) upstream of the FAST protein

404   open-reading frame. Following confirmation of correct assembly via DNA sequencing, the FAST

405   41BB-mCherry (pAF137) was digested and used as the base vector (**Figure 2B** and **Figure S1A-**

406   **B**) for development of FAST vectors with alternative fluorescent proteins. This was accomplished

407   by digestion of pAF137 with SalI and NheI and then inserting PCR-amplified coding sequences

408   for other fluorescent proteins using NEBuilder (**Tables S3-S4**).

409   Type I FAST (extracellular N-terminus, cytoplasmic C-terminus) protein vectors were

410   constructed by digestion of 41BB FAST vectors with NotI and either XmaI or SmaI (**Figure 2B**

411   and **Figure S1A-B**), and then inserting genes-of-interest (**Tables S2-4**). To create an Fc-tagged

412   FAST protein we fused the extracellular domain of devil CD80 to the Fc region of the devil IgG

413   (**Figure S1C**). The Fc region was amplified from a devil IgG plasmid provided by Lynn Corcoran

414   (Walter and Eliza Hall Institute of Medical Research). All secreted FAST proteins in this study

415   used their native signal peptides, except for 41BBL. 41BBL is a type II transmembrane protein in

416   which the signal peptide directly precedes the cytoplasmic and transmembrane domains of the

417   protein (cytoplasmic N-terminus, extracellular C-terminus). As type I FAST vectors cannot

418   accommodate this domain architecture, we developed an alternative base vector for type II

419   transmembrane FAST proteins (**Figure S1D**). To increase the probability of efficient secretion of

420   type II FAST proteins from CHO cells, we used the hamster IL-2 signal peptide (accession #

421   NM_001281629.1) at the N-terminus of the protein, followed by a SalI restriction site, mCherry,

422   an NheI restriction site, 6x-His tag, GSAGSAAGSGEF linker, TEV cleavage site, XmaI/SmaI

423   restriction site, the gene-of-interest, and a PmeI restriction site following the stop codon.

424   **General plasmid assembly, transformation, and sequencing**

425   Following transformation of assembled plasmids, colony PCR was performed as an initial

426   test of the candidate plasmids. Single colonies were inoculated directly into a OneTaq Hot Start

427   Quick-Load 2X Master Mix (NEB # M0488) with primers pSB_EF1a_seq.FOR

428   (atcttggttcattctcaagcctcag) and pSB_bGH_seq.REV (aggcacagtcgaggctgat). PCR was performed

429   with 60 °C annealing temperature for 25-35 cycles. Colonies yielding appropriate band sizes were

430   used to inoculate Luria broth with 100 μg/mL ampicillin for bacterial outgrowth overnight at 37

431   °C and 200 RPM. The plasmids were purified using standard plasmid kits and prepared for Sanger

432   sequencing using BigDye Terminator v3.1 Cycle Sequencing Kit (ThermoFisher # 4337455) with

433   pSB_EF1a_seq.FOR and pSB_bGH_seq.REV primers. The BigDye® Terminator was removed

434   using Agencourt CleanSEQ® (Beckman Coulter # A29151) before loading samples to an Applied

435   Biosystems® 3500XL Genetic Analyzer (Applied Biosystems) for sequencing by fluorescence-

436   based capillary electrophoresis.

437   **General cell culture conditions**

438   DFT1 cell line C5065 and DFT2 cell line JV were cultured at 35 °C with 5% CO_2 in cRF10

439   (10% complete RPMI (Gibco # 11875-093) with 2 mM L-glutamine, supplemented with 10% heat-

440   inactivated fetal bovine serum (FBS), and 1% antibiotic-antimycotic (ThermoFisher # 15240062).

441   RPMI without phenol red (Sigma # R7509) was used to culture FAST protein cell lines when

442   supernatants were collected for downstream flow cytometry assays. Devil peripheral blood cells

443   were cultured in cRF10 at 35 °C with 5% CO_2. CHO cells were cultured at 37 °C in cRF10 during

444   transfections and drug selection but were otherwise cultured at 35 °C in cRF5 (5% complete

445   RPMI). For production of purified recombinant proteins, stably transfected CHO cells were

446   cultured in suspension in spinner flasks in chemically defined, serum-free CHO Ex-Cell (Sigma #

447   14361C) media supplemented with 8 mM L-glutamine, 10 mM HEPES, 50 μM 2-ME, 1% (v/v)

448   antibiotic-antimycotic, and 1 mM sodium pyruvate and without hygromycin.

449   **Transfection and Generation of Recombinant Cell Lines**

450   Stable transfections of CHO and DFT cells were accomplished by adding 3 x 10^5 cells to

451   each well in 6-well plates in cRF10 and allowing the cells to adhere overnight. The next day, 2 μg

452   of plasmid DNA was added to 100 μL of PBS in microfuge tubes. Polyethylenimine (PEI) (linear,

453   MW 25,000; Polysciences # 23966-2) was diluted to 60 μg/mL in PBS and incubated for at least

454   two minutes. 100 μL of the PEI solution was added to the 100 μL of plasmid DNA in each tube to

455   achieve a 3:1 ratio of PEI:DNA. The solution was mixed by gentle pipetting and incubated at room

456   temperature for 15 minutes. Whilst the solution was incubating, the media on the CHO cells were

457   replaced with fresh cRF10. All 200 μL from each DNA:PEI mix was then added dropwise to the

458   CHO cells and gently rocked side-to-side and front-to-back to evenly spread the solution

459   throughout the well. The plates were then incubated overnight at 37 °C with 5% CO_2. The next

460   day the plates were inspected for fluorescence and then the media was removed and replaced with

461   cRF10 containing 1 mg/mL hygromycin (Sigma # H0654). The media was replaced with fresh

462   cRF10 1 mg/ml hygromycin every 2-3 days for the next seven days until selection was complete.

463   The cells were then maintained in 0.2 mg/mL hygromycin in cRF5 at 35 °C with 5% CO_2.

464   Supernatant was collected 2-3 weeks post-transfection and stored at 4 °C for two months to assess

465   stability of secreted FAST proteins.

Protein production and purification

467   16 days post-transfection the first batch of FAST protein cell lines were adapted to a 1:1

468   mix of cRF5 and chemically defined, serum free CHO Ex-cell media for 1-2 days to facilitate

469   adaptation of the adherent CHO cells to suspension culture in serum-free media. At least $5x10^7$

470   cells were then transferred to Proculture spinner flasks (Sigma # CLS45001L, CLS4500250) and

471   stirred at 75 RPM at 35 °C in 5% CO_2 on magnetic stirring platforms (Integra Bioscience #

472   183001). Cells were maintained at a density ranging from $5x10^5$ to $2x10^6$ cells/ml for 8-14 days.

473   Supernatant was collected every 2-3 days, centrifuged at 3200 RCF for 10 minutes, stored at 4 °C,

474   and then purified using the ÄKTA start protein purification system (GE Life Sciences #

475   29022094). The supernatant was diluted 1:1 with 20 mM sodium phosphate pH 7.4 and then

476   purified using HisTrap Excel columns (GE Life Sciences # 17-3712-05) according to the

477   manufacturer's instructions. Samples were passed through the columns using a flow rate of 2

478   mL/minute at 4 °C; all wash and elution steps were done at 1 mL/minute. Elution from HisTrap

479   columns (GE Life Sciences # 17-3712-05) was accomplished using 0.5 M imidazole and

480   fractionated into 1 ml aliquots using the Frac30 fraction collector (GE Life Sciences # 29023051).

481   Fluorescence of FAST proteins was checked via brief excitation (**Figure 2D**) on a blue light

482   transilluminator with an amber filter unit. In the case of mCherry chromogenic color was visible

483   (**Figure 2E**) without excitation. Fractions containing target proteins were combined and diluted to

484   15 mL with cold PBS, dialyzed (Sigma # PURX60005) in PBS at 4 °C, 0.22 μm sterile-filtered

485   (Millipore # SLGV033RS) and concentrated using Amicon Ultra centrifugal filter units (Sigma #

486   Z706345). The protein concentration was quantified using the 280 nm absorbance on a Nanodrop

487   spectrophotometer. Extinction coefficients using for each protein were calculated using the

488   ProtParam algorithm [81]. The proteins were then aliquoted into microfuge tubes and frozen at -80

489   °C until further use. The CTLA4-Fc-mCherry protein was designed, assembled, and tested

490   separately from the other FAST proteins and was tested directly in supernatant without

491   purification.

Preparation of CHO cells expressing full-length proteins for flow cytometry

493   CHO cells expressing full-length proteins were thawed in cRF10 and then maintained in

494   cRF5 with 0.2 mg/mL hygromycin. The adherent CHO cells were washed with PBS and incubated

495   with trypsin for 5 minutes at 37 °C to remove cells from the culture flask. Trypsin was diluted 5X

496   with cRF5 and centrifuged at 200 RCF for 5 minutes. Cells were resuspended in cRF5, counted

497   (viability > 95% in all cases), and resuspended and aliquoted for assays as described below.

Initial staining of CHO cells with 41BB FAST protein supernatants (without chloroquine)

499   Supernatants (cRF5) were collected from CHO cells expressing devil 41BB-extracellular

500   domain fused to either mCherry (pAF137), mCitrine (pAF138), mOrange (pAF164), mBFP

501   (pAF139), mAzurite (pAF160), mCerulean3 (pAF161), or mNeptune2 (pAF163) (**Tables S2-4**).

502   The supernatant was spun for 10 minutes at 3200 RCF to remove cells and cellular debris, and

503   then stored at 4 °C until further use. CHO cells expressing devil 41BBL (CHO.pAF56) and

504   untransfected CHO cells were prepared as described above. Flow cytometry tubes were loaded

505   with 5 x 10^4 target CHO cells/well in cRF5, centrifuged 500 RCF for 3 minutes, and then

506   resuspended in 200 μL of supernatant from the 41BB FAST cell lines (n=1/treatment). The tubes

507   were then incubated for 15 minutes at 4 °C, centrifuged at 500 RCF for 3 minutes, resuspended in

508   400 μL of cold FACS buffer, and stored on ice until the data were acquired on a Beckman-Coulter

509   Astrios flow cytometer (**Figure 2C**). All flow cytometry data was analyzed using FCS Express 6

510   Flow Cytometry Software version 6 (Denovo Software).

511   **Staining CHO cells with FAST protein supernatants (without chloroquine)**

512   U-bottom 96-well plates were loaded with 1 x 10^5 target CHO cells/well in cRF5,

513   centrifuged 500 RCF for 3 minutes, and then resuspended in 175 μL of cRF5 supernatant from

514   FAST cell lines collected 11 days after transfection (n=1/treatment). The plates were then

515   incubated for 30 minutes at room temperature, centrifuged at 500 RCF for 3 minutes, resuspended

516   in 200 μL of cold FACS buffer, centrifuged again and fixed with FACS fix buffer (PBS, 0.02%

517   NaN3, 0.4% formalin, 10g/L glucose). The cells were transferred to tubes, diluted with FACS

518   buffer and analyzed on a Beckman-Coulter Astrios flow cytometer (**Figure S2**).

519   **Staining CHO cells with purified FAST proteins (with chloroquine)**

520   Purified FAST proteins were diluted to 20 μg/mL in cRF5, aliquoted into V-bottom 96-

521   well transfer plates, and then stored at 37 °C until target cells were ready for staining. Target cells

522   were resuspended in cRF5 with 100 μM chloroquine and 100,000 cells/well were aliquoted into

523   U-bottom 96-well plates. 100 μL of the diluted FAST proteins (n=1/treatment, 2

524   timepoints/treatment) were then transferred from the V-bottom plates into the U-bottom 96-well

525   plates containing target cells. The final volumes and concentrations were 200 μL/well in cRF5

526   with 50 μM chloroquine and 2 μg/well of FAST proteins. One set of plates was incubated at 37 °C

527   for 30 minutes and another set of plates was incubated at 37 °C overnight. The cells were then

528   centrifuged 500 RCF for 3 minutes, the media decanted, and incubated for 5 minutes with 100 μL

529   of trypsin to dislodge adherent cells. The cells were then washed with 200 μL of cold FACS buffer,

530   fixed, resuspended in cold FACS buffer, and transferred to tubes for analysis on the Astrios flow

531   cytometer (**Figure 3B**).

532 Staining CHO cells with FAST supernatants (with chloroquine)

533   The protocol for using FAST protein supernatants was the same above as the preceding

534 experiment except for the modifications described here. Supernatants were collected 2-3 weeks

535 post-transfection, centrifuged at 3200 RCF for 10 minutes, and stored at 4 °C for 2 months. Prior

536 to staining for flow cytometry, the supernatant was 0.22 μm filtered. Supernatant was then loaded

537 into V-bottom 96-well plates to facilitate rapid transfer to staining plates and stored at 37 °C until

538 target cells were ready for staining. Target cells were prepared as described above except for being

539 diluted in cRF5 with 100 μM chloroquine. 2×10^5 cells/well (100 μL) were then loaded into U-

540 bottom 96-well plates. 100 μL of FAST protein supernatant (n=1/treatment) was then transferred

541 from the V-bottom plates to achieve 50 μM chloroquine and the cells were then incubated at 37

542 °C for 60 minutes. The plates were then washed, fixed, and analyzed on the Astrios flow cytometer

543 (**Figure S3**). A similar procedure was used for staining stably-transfected DFT cells with CTLA4-

544 Fc-mCherry, except that the supernatant was used fresh (**Figure 4D**).

545 Coculture assay with full-length target and FAST protein CHO cell lines (with chloroquine)

546   CHO cells expressing full-length CTLA4 with a C-terminal mCitrine, and CHO cells

547 expressing full-length 41BB or 41BBL were labelled with 5 μM CFSE; CFSE and mCitrine were

548 analyzed using the same excitation laser (488 nm) and emission filters (513/26 nm). 1×10^5 FAST

549 protein-secreting cells were mixed with 1×10^5 target cells in cRF5 with 50 μM chloroquine and

550 incubated overnight at 37 °C in 96-well U-bottom plates (**Figure 4A**). The next day the cells were

551 rinsed with PBS, trypsinized, washed, fixed, and resuspended in FACS buffer prior to running

552 flow cytometry. Cells were gated on forward and side scatter (FSC x SSC) and for singlets (FSC-

553 H x FSC-A). (**Figure 4B).** Data shown in **Figure 4C** is representative of n=3 technical

554   replicates/treatment. Data was collected using a Beckman Coulter MoFlo Astrios and analyzed

555   using FCS Express.

Analysis of checkpoint molecule expression in DFT cells and Tasmanian devil tissues

557   RNAseq data was generated during previous experiments, aligned against the reference

558   Tasmanian devil genome Devil_ref v7.0 (GCA_000189315.1) and summarised into normalized

559   read counts as previously described [34,35]. RPKM-normalized read counts were produced in R using

560   edgeR[82]. Genes were ranked from highest RPKM-normalized count to lowest RPKM-normalized

561   count, and a heat map was produced for the genes of interest using the heatmap.2 function of

562   gplots. Heatmap color represents gene ranking among 18,788 predicted protein-coding genes in

563   the reference genome.

Staining DFTs cell with CD200/R FAST proteins

565   50,000 DFT cells/well were aliquoted into u-bottom 96-well plates, washed with 150 μL

566   of cRF10, and resuspended in 100 μL of warm cRF10 containing 100 μM chloroquine. 5 μg of

567   FAST protein/well was then added and mixed by pipetting. The plates were then incubated at 37

568   °C for 30 minutes. The cells were then transferred to microfuge tubes without washing, stored on

569   ice, and analyzed on a Beckman Coulter MoFlo Astrios (n=2/treatment).

Polyclonal antibody development

571   CD200 and 41BB FAST proteins were digested overnight with TEV protease (Sigma #

572   T4455) at 4 °C in PBS. The cleaved linker and 6x-His tag were then removed using a His SpinTrap

573   kit (GE Healthcare # 28-9321-71). Digested proteins in PBS were diluted 1:1 in Squalvax (Oz

574   Biosciences # SQ0010) to a final concentration of 0.1 μg/μL and was mixed using interlocked

575   syringes to form an emulsion. Immunization of BALB/c mice for antibody production was

576   approved by the University of Tasmania Animal Ethics Committee (# A0014680). Pre-immune

577   sera were collected prior to subcutaneous immunization with at least 50 µL of the emulsion. On

578   day 14 post-immunization the mice were boosted using a similar procedure. On day 50 the mice

579   received a booster with proteins in IFAVax (Oz Biosciences # IFA0050); mice immunized with

580   CD200 again received subcutaneous injections, whereas 41BB mice received subcutaneous and

581   intraperitoneal injections. Pre-immune and sera collected after 3X immunizations were then tested

582   by flow cytometry against CHO cells expressing either 41BB or CD200. CHO cells were prepared

583   as described above and $2x10^5$ cells were incubated with mouse serum diluted 1:200 in PBS for 30

584   minutes at 4 °C. The cells were then washed 2X and stained with 50 µL of anti-mouse IgG

585   AlexaFluor 647 diluted 1:1000 in FACS buffer. The cells were then washed 2X, stained with DAPI

586   to identify live cells, and analyzed on a Cyan ADP flow cytometer (**Figure 5C**). CD200 and 41BB

587   expression on DFT cells was tested using a procedure similar to the CHO cell staining, except the

588   sera used was collected after 4X immunizations and was diluted 1:500 and analyzed on the BD

589   FACSCanto II (**Figure 5D**).

590   **Purification of antibodies from normal mouse serum (NMS) and anti-CD200 serum**

591   Approximately 200 µL of normal mouse serum or anti-CD200 serum day 157 (after 4X

592   immunizations) were purified using a protein G SpinTrap (GE Healthcare # 28-4083-47) according

593   to the manufacturer's instrutions. Serum was diluted 1:1 with 20 mM sodium phosphate, pH 7.0

594   binding buffer, eluted with 0.1 M glycine-HCl, pH 2.7, and the pH was neutralized with 0.1 M

595   glycine-HCl, pH 2.7. The eluted antibodies were then concentrated using an Amicon Ultra 0.5

596   centrifugal until (Merck # UFC500308) by centrifuging at 14,000 RCF for 30 minutes at 4 °C and

597   then washing the antibodies with 400 µL of PBS twice. The protein concentration was then

598   quantified on a Nanodrop spectrophotometer at 280 nm using the extinction coefficients for IgG.

599   **Testing CD200 expression on DFT cells that overexpress CD200R1**

600   50,000 DFT cells/well were aliquoted into u-bottom 96-well plates and washed with 200

601   μL of cold FACS buffer. Purified polyclonal anti-CD200 was diluted to 2.5 μg/mL in cold FACS

602   buffer and the cells in appropriate wells were resuspend in 100 μL/well (0.25 μg/well) diluted

603   antibody; wells that did not receive antibody were resuspended in 100 μL of FACS buffer. The

604   cells were incubated on ice for 20 minutes and then washed with 200 μL of FACS buffer. Whilst

605   incubating, anti-mouse IgG-AF647 was diluted to 1 μg/mL in cold FACS buffer and then used to

606   resuspend cells in the appropriate wells. The plates were incubated on ice for 20 minutes, then

607   washed with 100 μL of cold FACS buffer. The cells were then resuspended in 200 μL of FACS

608   fix and incubated on a rocking platform at room temp for 15 minutes. The cells were then

609   centrifuged 500 RCF for 3 minutes at 4 °C, resuspended in 200 μL FACS buffer and stored at 4

610   °C until they were analyzed on a FACSCanto II (n=2/treatment).

611   **Isolation of devil peripheral blood mononuclear cells**

612   Blood collection from Tasmanian devils was approved by the University of Tasmania

613   Animal Ethics Committee (permit # A0014599) and the Tasmanian Department of Primary

614   Industries, Parks, Water and Environment (DPIPWE). Blood was collected from the jugular vein

615   and stored in EDTA tubes for transport to the lab. Blood was processed within three hours by

616   diluting 1:1 with serum-free RPMI and then layering onto Histopaque (Sigma # 10771) before

617   centrifuging at 400 RCF for 30 minutes. The interface containing the peripheral blood

618   mononuclear cells was then collected using a transfer pipette, diluted with 50 mL of serum-free

619   RPMI and centrifuged for 5 minutes at 500 RCF. Cells were washed with again with cRF10 and

620   then either used fresh or stored at -80 °C until further use.

621   **Detecting DFT2 cells in PBMC using CD200**

622   Frozen devil PBMC were thawed and cultured in cRF10 at 35 °C with 5% CO_2 for 2 hours,

623   cells were then washed in FACS buffer, counted and $3x10^5$ PBMC cells used per sample. DFT2.JV

624   cells were removed from culture flasks, counted, and $2x10^5$ cells used per sample. Samples were

625   incubated with 50 μL normal goat serum (Thermo Cat # 01-6201) diluted 1:200 in FACS buffer

626   for 15 minutes at 4 °C, 50 μL of anti-CD200 serum diluted 1:100 was added (1:200 final) for 30

627   minutes at 4 °C. Cells were then washed 2X and stained with 50 μL of anti-mouse IgG AlexaFluor

628   647 diluted to 1 μg/mL in FACS buffer for 30 minutes at 4 °C. The cells were then washed 2X,

629   stained with DAPI (Sigma Cat # D9542) to identify live cells, and analyzed on the BD FACSCanto

630   II. PBMC and DFT cells were run separately then PBMC and DFT2 mixed at a ratio of 10:1 by

631   volume for the combined samples (n=1/treatment) (**Figure S4A**). The experiment was repeated

632   (n=1/treatment), except that PBMCs and DFT cells were mixed at a 5:1 ratio (**Figure S4B**).

633   **Staining of DFT cells in devil whole blood**

634   DFT1.C5065 and DFT2.JV cells were labelled with 5 μM CellTrace violet (CTV) and

635   cultured for three days at 37 °C. On the day of the assays peripheral blood from one devil was

636   collected and stored at ambient temp for less than three hours. 100 μL of whole blood was aliquoted

637   into 15 mL tubes and stored at ambient temperature whilst DFT cells were prepared. The media

638   on CTV-labeled DFT cells were decanted and the cells were detached from the flask by incubating

639   in 2.5 mL of TrypLE Select for 5 minutes at 37 °C. The cells were washed with cRF10,

640   resuspended in cRF10, and counted. DFT cells were then diluted to $1x10^4$ cells/mL in cRF10 and

641   100 μL were aliquoted into appropriate 15 mL tubes containing 100 μL of whole blood. 1 μL of

642   purified anti-CD200 (0.5 μg/tube) was diluted into the appropriate tubes and incubated for 15

643   minutes at ambient temperature. Next, 0.5 μg/tube of anti-mouse IgG AF647 was added to each

644   tube. Note: 0.5 μL (0.5 μg) of concentrated secondary antibody was accidentally added directly to

645   the tube for the data shown in the top row and middle column of **Figure S5A;** for all other tubes

646   the secondary antibody was diluted 1:20 in PBS and 10 μL was added to each tube. The cells were

647   then incubated for 15 minutes at ambient temperature. The cells were then diluted in 1 mL

648   ammonium chloride red blood cell (RBC) lysis buffer (150 mM NH_4Cl, 10 mM $KHCO_3$, 0.1 mM

649   EDTA disodium (Na_2-$2H_2O$)) and mixed immediately gently pipetting five times. The cells were

650   incubated at ambient temperature for 10 minutes and then diluted with 5 mL of PBS and

651   centrifuged 500 RCF for 3 minutes. Some tubes contained residual RBCs, so the pellet was

652   vigorously resuspended in 5 mL of RBC lysis buffer, incubated for 5 minutes, diluted with 5 mL

653   of cold FACS buffer, and centrifuged 500 RCF for 3 minutes. The cells were then resuspended in

654   250 μL of FACS buffer and stored on ice until analysis on a Beckman Coulter MoFlo Astrios

655   (n=1/treatment). Data were analyzed in FCS Express version 6 (**Figure S5**).

656   The experiment above was repeated with the following modifications. DFT cells were

657   labelled with 5 μM of CFSE and incubated for two days at 37 °C. On the day of the assays fresh

658   blood was collected from two devils. Purified anti-CD200 and NMS were labeled with Zenon

659   mouse IgG AF647 (ThermoFisher # Z25008) and blocked with the Zenon blocking agent. $1x10^4$

660   CFSE-labeled DFT cells were diluted directly into 100 μL of whole blood in 15 mL tubes and 12

661   μL (2 μL antibody, 5 μL labeling agent, 5 μL blocking agent) of Zenon AF647-labeled purified

662   NMS or anti-CD200 were added directly to the cells. The cells were incubated for 30 minutes at

663   ambient temperature. The cells were then gently resuspended in 2.5 mL of RBC lysis buffer and

664   incubated for 10 minutes at ambient temperature. The cells were diluted with 10 mL of PBS and

665   centrifuged 500 RCF for 3 minutes. The cells were resuspended in 1.5 mL of RBC lysis buffer and

666   incubated for another 10 minutes to lyse residual RBCs. The tubes were then resuspended in 9 mL

667   of cRF10 and centrifuged 500 RCF for 3 minutes. The cells were resuspended in 350 μL of cold

668   FACS buffer containing 200 ng/mL of DAPI and stored on ice until analysis on a Beckman Coulter

669   MoFlo Astrios (n=1/treatment for n = 2 devils) (**Figure 6**).

670

ACKNOWLEDGMENTS

684

AUTHOR CONTRIBUTIONS

686   ASF designed the study; ALP, ASF, CEBO, PRL, and PRM developed the technology; ASF,

687   CEBO, PRL, PRM, JMD, and TLP performed the experiments; ALP performed bioinformatic

688   analyses; ALP, ASF, JMD and PRL created the figures; ALP, ASF, PRL, JMD, TLP, and GMW

689   analyzed the data; ASF wrote the manuscript and all authors edited the manuscript.

690

691 **AVAILABILITY OF DATA AND MATERIALS**

692 All data are included with the paper. The FAST base vectors (pAF92.3 pAF112.7, pAF123.1,

693 pAF138.7, pAF139.2, pAF160.1, pAF161.3, pAF163.1, pAF164.3, pAF197) have been submitted

694 to Addgene for distribution c(deposit # 77504).

695

696 **CONFLICT OF INTEREST**

697 The authors received funding from Nexvet Australia Pty. Ltd for related studies.

698

REFERENCES

1   Albuquerque TAF, Drummond do Val L, Doherty A, de Magalhães JP. From humans to hydra: patterns of cancer across the tree of life. *Biol Rev* 2018; **93**: 1715–1734.

2   Abu-Helil B, Van Der Weyden L. Metastasis in the wild: investigating metastasis in non-laboratory animals. *Clin Exp Metastasis* 2019. doi:10.1007/s10585-019-09956-3.

3   Olds JE, Burrough ER, Fales-Williams AJ, Lehmkuhl A, Madson D, Patterson AJ *et al.* Retrospective Evaluation of Cases of Neoplasia in a Captive Population of Egyptian Fruit Bats (Rousettus Aegyptiacus). *J Zoo Wildl Med* 2015; **46**: 325–332.

4   Chu PY, Zhuo YX, Wang FI, Jeng CR, Pang VF, Chang PH *et al.* Spontaneous neoplasms in zoo mammals, birds, and reptiles in Taiwan - A 10-year survey. *Anim Biol* 2012; **62**: 95–110.

5   Deus A De, Alves F, Siqueira DB De, Rameh-de-albuquerque LC. Breast Carcinoma with Pulmonary Metastasis in Armadillo (Eupharactus sexcinctus). *Acta Sci Vet* 2018; **46**: 1–5.

6   Kruse TN, Garner MM, Bonar CJ. A Retrospective Study of Pathologic Findings in Captive Rock Hyrax (Procavia Capensis) in the United States. *J Zoo Wildl Med* 2015; **46**: 798–805.

7   Effron M, Griner L, Benirschke K. Nature and rate of neoplasia found in captive wild mammals, birds, and reptiles at necropsy. *J Natl Cancer Inst* 1977; **59**: 185–198.

8   Ratcliffe HL. Incidence and nature of tumors in captive wild mammals and birds. *Am J Cancer* 1933; **17**: 116–135.

9   Priester WA, Mantel N. Occurrence of tumors in domestic animals. Data from 12 United States and Canadian colleges of veterinary medicine. *J Natl Cancer Inst* 1971; **47**: 1333–1344.

33

722   10   Howlader N, Noone A, Krapcho M, Miller D, Brest A, Yu M *et al.* SEER Cancer

723   Statistics Review, 1975-2016. Bethesda, MD, United States, 2016.

724   11   Griner LA. Neoplasms in Tasmanian devils (Sarcophilus harrisii). *J Natl Cancer Inst*

725   1979; **62**: 589–595.

726   12   Peck SJ, Michael SA, Knowles G, Davis A, Pemberton D. Causes of mortality and severe

727   morbidity requiring euthanasia in captive Tasmanian devils (Sarcophilus harrisii) in

728   Tasmania. *Aust Vet J* 2019; **97**: 89–92.

729   13   Pearse A-M, Swift K. Allograft theory: transmission of devil facial-tumour disease.

730   *Nature* 2006; **439**: 549.

731   14   Pye RJ, Pemberton D, Tovar C, Tubio JMC, Dun KA, Fox S *et al.* A second transmissible

732   cancer in Tasmanian devils. *Proc Natl Acad Sci* 2016; **113**: 374–379.

733   15   Murgia C, Pritchard JK, Kim SY, Fassati A, Weiss RA. Clonal Origin and Evolution of a

734   Transmissible Cancer. *Cell* 2006; **126**: 477–487.

735   16   Fleming JM, Creevy KE, Promislow DEL. Mortality in North American Dogs from 1984

736   to 2004: An Investigation into Age-, Size-, and Breed-Related Causes of Death. *J Vet*

737   *Intern Med* 2011; **25**: 187–198.

738   17   Lazenby BT, Tobler MW, Brown WE, Hawkins CE, Hocking GJ, Hume F *et al.* Density

739   trends and demographic signals uncover the long-term impact of transmissible cancer in

740   Tasmanian devils. *J Appl Ecol* 2018; **55**: 1368–1379.

741   18   James S, Jennings G, Kwon YM, Stammnitz M, Fraik A, Storfer A *et al.* Tracing the rise

742   of malignant cell lines: distribution, epidemiology and evolutionary interactions of two

743   transmissible cancers in Tasmanian devils. *Evol Appl* 2019; : eva.12831.

744   19   Siddle H V., Kreiss A, Tovar C, Yuen CK, Cheng Y, Belov K *et al.* Reversible epigenetic

down-regulation of MHC molecules by devil facial tumour disease illustrates immune escape by a contagious cancer. *Proc Natl Acad Sci* 2013; **110**: 5103–8.

20   Yoshihama S, Roszik J, Downs I, Meissner TB, Vijayan S, Chapuy B *et al.* NLRC5/MHC class I transactivator is a target for immune evasion in cancer. *Proc Natl Acad Sci* 2016; **113**: 5999–6004.

21   Caldwell A, Coleby R, Tovar C, Stammnitz MR, Mi Kwon Y, Owen RS *et al.* The newly-arisen devil facial tumour disease 2 (DFT2) reveals a mechanism for the emergence of a contagious cancer. *Elife* 2018; **7**. doi:10.7554/eLife.35314.

22   Stammnitz MR, Coorens THH, Gori KC, Hayes D, Fu B, Wang J *et al.* The Origins and Vulnerabilities of Two Transmissible Cancers in Tasmanian Devils. *Cancer Cell* 2018; **33**: 607-619.e15.

23   Topalian SL, Hodi FS, Brahmer JR, Gettinger SN, Smith DC, McDermott DF *et al.* Safety, Activity, and Immune Correlates of Anti–PD-1 Antibody in Cancer. *N Engl J Med* 2012; **366**: 2443–2454.

24   Larkin J, Chiarion-Sileni V, Gonzalez R, Grob JJ, Cowey CL, Lao CD *et al.* Combined Nivolumab and Ipilimumab or Monotherapy in Untreated Melanoma. *N Engl J Med* 2015; **373**: 23–34.

25   Flies AS, Bruce Lyons A, Corcoran LM, Papenfuss AT, Murphy JM, Knowles GW *et al.* PD-L1 is not constitutively expressed on tasmanian devil facial tumor cells but is strongly upregulated in response to IFN-γ and can be expressed in the tumor microenvironment. *Front Immunol* 2016; **7**: 581.

26   Ong CEB, Lyons AB, Woods GM, Flies AS. Inducible IFN-γ Expression for MHC-I Upregulation in Devil Facial Tumor Cells. *Front Immunol* 2018; **9**: 3117.

768 27 Flies AS, Blackburn NB, Lyons AB, Hayball JD, Woods GM. Comparative analysis of

769   immune checkpoint molecules and their potential role in the transmissible tasmanian devil

770   facial tumor disease. *Front Immunol* 2017; **8**: 513.

771 28 World Health Organization (WHO). WHO R&D Blueprint for action to prevent

772   epidemics. World Health Organization, 2016http://www.who.int/blueprint/en/ (accessed 1

773   May2018).

774 29 Shaner NC, Campbell RE, Steinbach PA, Giepmans BNG, Palmer AE, Tsien RY.

775   Improved monomeric red, orange and yellow fluorescent proteins derived from

776   Discosoma sp. red fluorescent protein. *Nat Biotechnol* 2004; **22**: 1567–72.

777 30 Cabantous S, Terwilliger TC, Waldo GS. Protein tagging and detection with engineered

778   self-assembling fragments of green fluorescent protein. *Nat Biotechnol* 2005; **23**: 102–

779   107.

780 31 Cha HJ, Dalal NN, Bentley WE. Secretion of human interleukin-2 fused with green

781   fluorescent protein in recombinant Pichia pastoris. *Appl Biochem Biotechnol* 2005; **126**:

782   1–11.

783 32 Duellman T, Burnett J, Yang J. Quantitation of secreted proteins using mCherry fusion

784   constructs and a fluorescent microplate reader. *Anal Biochem* 2015; **473**: 34–40.

785 33 Kammertoens T, Friese C, Arina A, Idel C, Briesemeister D, Rothe M *et al.* Tumour

786   ischaemia by interferon-γ resembles physiological blood vessel regression. *Nature* 2017;

787   **545**: 98–102.

788 34 Patchett AL, Wilson R, Charlesworth JC, Corcoran LM, Papenfuss AT, Lyons AB *et al.*

789   Transcriptome and proteome profiling reveals stress-induced expression signatures of

790   imiquimod-treated Tasmanian devil facial tumor disease (DFTD) cells. *Oncotarget* 2018;

791   **9**: 15895–15914.

792   35   Patchett AL, Coorens THH, Darby J, Wilson R, McKay MJ, Kamath KS *et al.* Two of a

793   kind: transmissible Schwann cell cancers in the endangered Tasmanian devil (Sarcophilus

794   harrisii). *Cell Mol Life Sci* 2019; : 1–12.

795   36   Seglen PO, Grinde B, Solheim AE. Inhibition of the Lysosomal Pathway of Protein

796   Degradation in Isolated Rat Hepatocytes by Ammonia, Methylamine, Chloroquine and

797   Leupeptin. *Eur J Biochem* 1979; **95**: 215–225.

798   37   Qureshi OS, Zheng Y, Nakamura K, Attridge K, Manzotti C, Schmidt EM *et al.* Trans-

799   endocytosis of CD80 and CD86: a molecular basis for the cell extrinsic function of

800   CTLA-4. *Science* 2011; **332**: 600–603.

801   38   van den Bremer ET, Beurskens FJ, Voorhorst M, Engelberts PJ, de Jong RN, van der

802   Boom BG *et al.* Human IgG is produced in a pro-form that requires clipping of C-terminal

803   lysines for maximal complement activation. *MAbs* 2015; **7**: 672–680.

804   39   Patchett AL, Latham R, Brettingham-Moore KH, Tovar C, Lyons AB, Woods GM. Toll-

805   like receptor signaling is functional in immune cells of the endangered Tasmanian devil.

806   *Dev Comp Immunol* 2015; **53**: 123–133.

807   40   Love JE, Thompson K, Kilgore MR, Westerhoff M, Murphy CE, Papanicolau-Sengos A

808   *et al.* CD200 Expression in Neuroendocrine Neoplasms. *Am J Clin Pathol* 2017; **148**:

809   236–242.

810   41   Murchison EP, Tovar C, Hsu A, Bender HS, Kheradpour P, Rebbeck CA *et al.* The

811   Tasmanian devil transcriptome reveals schwann cell origins of a clonally transmissible

812   cancer. *Science* 2010; **327**: 84–87.

813   42   Haile ST, Bosch JJ, Agu NI, Zeender AM, Somasundaram P, Srivastava MK *et al.* Tumor

814   cell programmed death ligand 1-mediated T cell suppression is overcome by coexpression

815   of CD80. *J Immunol* 2011; **186**: 6822–9.

816 43 Sugiura D, Maruhashi T, Okazaki I, Shimizu K, Maeda TK, Takemoto T *et al.* Restriction

817   of PD-1 function by *cis* -PD-L1/CD80 interactions is required for optimal T cell

818   responses. *Science* 2019; : eaav7062.

819 44 Moertel CL, Xia J, LaRue R, Waldron NN, Andersen BM, Prins RM *et al.* CD200 in CNS

820   tumor-induced immunosuppression: The role for CD200 pathway blockade in targeted

821   immunotherapy. *J Immunother Cancer* 2014; **2**: 46.

822 45 Challagundla P, Medeiros LJ, Kanagal-Shamanna R, Miranda RN, Jorgensen JL.

823   Differential Expression of CD200 in B-Cell Neoplasms by Flow Cytometry Can Assist in

824   Diagnosis, Subclassification, and Bone Marrow Staging. *AJCP / Orig Artic Am J Clin*

825   *Pathol* 2014; **142**: 837–844.

826 46 Spacek M, Karban J, Radek M, Babunkova E, Kvasnicka J, Jaksa R *et al.* CD200

827   Expression Improves Differential Diagnosis Between Chronic Lymphocytic Leukemia

828   and Mantle Cell Lymphoma. *Blood* 2014; **124**.

829 47 Saksena A, Yin CC, Xu J, Li J, Zhou J, Wang SA *et al.* CD23 expression in mantle cell

830   lymphoma is associated with CD200 expression, leukemic non-nodal form, and a better

831   prognosis. *Hum Pathol* 2019; **89**: 71–80.

832 48 Loh R, Hayes D, Mahjoor A, O'Hara A, Pyecroft S, Raidal S. The immunohistochemical

833   characterization of devil facial tumor disease (DFTD) in the Tasmanian Devil

834   (Sarcophilus harrisii). *Vet Pathol* 2006; **43**: 896–903.

835 49 Yao S, Zhu Y, Zhu G, Augustine M, Zheng L, Goode DJ *et al.* B7-h2 is a costimulatory

836   ligand for CD28 in human. *Immunity* 2011; **34**: 729–740.

837 50 Wang J, Sanmamed MF, Datar I, Su TT, Ji L, Sun J *et al.* Fibrinogen-like Protein 1 Is a

838 Major Immune Inhibitory Ligand of LAG-3. *Cell* 2018; **0**.

839 doi:10.1016/J.CELL.2018.11.010.

840 51 Aricescu AR, Lu W, Jones EY. A time- and cost-efficient system for high-level protein

841 production in mammalian cells. *Acta Crystallogr Sect D Biol Crystallogr* 2006; **62**: 1243–

842 1250.

843 52 Consortium SG, Biologiques A et F des M, Center BSG, Consortium CSG, Innovation IC

844 for S and F, Center ISP *et al.* Protein production and purification. *Nat Methods* 2008; **5**:

845 135.

846 53 Jayapal KP, Wlaschin KF, Hu WS, Yap MGS. Recombinant protein therapeutics from

847 CHO cells - 20 years and counting. *Chem Eng Prog* 2007; **103**: 40–47.

848 54 Atfy M. CD200 Suppresses the Natural Killer Cells and Decreased its Activity in Acute

849 Myeloid Leukemia Patients. *J Leuk* 2015; **3**.https://www.omicsonline.org/open-

850 access/cd200-suppresses-the-natural-killer-cells-and-decreased-its-activity-in-

851 acutemyeloid-leukemia-patients-2329-6917-1000190.pdf (accessed 18 Apr2019).

852 55 Coles SJ, Man S, Hills R, Wang EC, Burnett A, Darley RL *et al.* Over-Expression of

853 CD200 In Acute Myeloid Leukemia Mediates the Expansion of Regulatory T-

854 Lymphocytes and Directly Inhibits Natural Killer Cell Tumor Immunity. *Blood* 2015; **116**:

855 491.

856 56 Coles SJ, Wang ECY, Man S, Hills RK, Burnett AK, Tonks A *et al.* CD200 expression

857 suppresses natural killer cell function and directly inhibits patient anti-tumor response in

858 acute myeloid leukemia. *Leukemia* 2011; **25**: 792–9.

859 57 Gorczynski RM, Chen Z, Khatri I, Yu K. Graft-infiltrating cells expressing a CD200

860 transgene prolong allogeneic skin graft survival in association with local increases in

861 Foxp3 +Treg and mast cells. *Transpl Immunol* 2011; **25**: 187–193.

862 58 Gorczynski RM, Chen Z, He W, Khatri I, Sun Y, Yu K *et al.* Expression of a CD200

863 transgene is necessary for induction but not maintenance of tolerance to cardiac and skin

864 allografts. *J Immunol* 2009; **183**: 1560–1568.

865 59 Gorczynski L, Chen Z, Hu J, Kai Y, Lei J, Ramakrishna V *et al.* Evidence That an OX-2-

866 Positive Cell Can Inhibit the Stimulation of Type 1 Cytokine Production by Bone

867 Marrow-Derived B7-1 (and B7-2)-Positive Dendritic Cells. *J Immunol* 1999; **162**: 774–

868 781.

869 60 Harding J, Vintersten-Nagy K, Shutova M, Yang H, Tang JK, Massumi M *et al.* Induction

870 of long-term allogeneic cell acceptance and formation of immune privileged tissue in

871 immunocompetent hosts. Cold Spring Harbor Laboratory, 2019 doi:10.1101/716571.

872 61 Jenmalm MC, Cherwinski H, Bowman EP, Phillips JH, Sedgwick JD. Regulation of

873 Myeloid Cell Function through the CD200 Receptor. *J Immunol* 2014; **176**: 191–199.

874 62 Tovar C, Pye RJ, Kreiss A, Cheng Y, Brown GK, Darby J *et al.* Regression of devil facial

875 tumour disease following immunotherapy in immunised Tasmanian devils. *Sci Rep* 2017;

876 **7**: 43827.

877 63 Pye R, Patchett A, McLennan E, Thomson R, Carver S, Fox S *et al.* Immunization

878 strategies producing a humoral IgG immune response against devil facial tumor disease in

879 the majority of Tasmanian devils destined for wild release. *Front Immunol* 2018; **9**: 259.

880 64 Olin MR, Ampudia-Mesias E, Pennell CA, Sarver A, Chen CC, Moertel CL *et al.*

881 Treatment combining CD200 immune checkpoint inhibitor and tumor-lysate vaccination

882 after surgery for pet dogs with high-grade glioma. *Cancers (Basel)* 2019; **11**: 137.

883 65 Zhang S, Phillips JH. Identification of tyrosine residues crucial for CD200R-mediated

884   inhibition of mast cell activation. *J Leukoc Biol* 2005; **79**: 363–368.

885 66 Hatherley D, Lea SM, Johnson S, Barclay AN. Structures of CD200/CD200 receptor

886   family and implications for topology, regulation, and evolution. *Structure* 2013; **21**: 820–

887   832.

888 67 Luo ZX, Yuan CX, Meng QJ, Ji Q. A Jurassic eutherian mammal and divergence of

889   marsupials and placentals. *Nature* 2011; **476**: 442–445.

890 68 Wong KK, Khatri I, Shaha S, Spaner DE, Gorczynski RM. The role of CD200 in

891   immunity to B cell lymphoma. *J Leukoc Biol* 2010; **88**: 361–372.

892 69 Caserta S, Nausch N, Sawtell A, Drummond R, Barr T, MacDonald AS *et al.* Chronic

893   infection drives expression of the inhibitory receptor CD200R, and its ligand CD200, by

894   mouse and human CD4 T cells. *PLoS One* 2012; **7**: e35466.

895 70 Foster-Cuevas M, Westerholt T, Ahmed M, Brown MH, Barclay AN, Voigt S.

896   Cytomegalovirus e127 protein interacts with the inhibitory CD200 receptor. *J Virol* 2011;

897   **85**: 6055–9.

898 71 Foster-Cuevas M, Wright GJ, Puklavec MJ, Brown MH, Barclay AN. Human herpesvirus

899   8 K14 protein mimics CD200 in down-regulating macrophage activation through CD200

900   receptor. *J Virol* 2004; **78**: 7667–76.

901 72 Alves JM, Carneiro M, Cheng JY, Matos AL de, Rahman MM, Loog L *et al.* Parallel

902   adaptation of rabbit populations to myxoma virus. *Science* 2019; : eaau7285.

903 73 Barclay AN, Hatherley D. The Counterbalance Theory for Evolution and Function of

904   Paired Receptors. *Immunity* 2008; **29**: 675–678.

905 74 Tovar C, Obendorf D, Murchison EP, Papenfuss AT, Kreiss A, Woods GM. Tumor-

906   specific diagnostic marker for transmissible facial tumors of tasmanian devils:

907   Immunohistochemistry studies. *Vet Pathol* 2011; **48**: 1195–1203.

908 75 Marx V. Calling the next generation of affinity reagents. *Nat Methods* 2013; **10**: 829–833.

909 76 Grabherr MG, Haas BJ, Yassour M, Levin JZ, Thompson DA, Amit I *et al.* Full-length

910   transcriptome assembly from RNA-Seq data without a reference genome. *Nat Biotechnol*

911   2011; **29**: 644–52.

912 77 Kowarz E, Löscher D, Marschalek R. Optimized Sleeping Beauty transposons rapidly

913   generate stable transgenic cell lines. *Biotechnol J* 2015; **10**: 647–653.

914 78 Mátés L, Chuah MKL, Belay E, Jerchow B, Manoj N, Acosta-Sanchez A *et al.* Molecular

915   evolution of a novel hyperactive Sleeping Beauty transposase enables robust stable gene

916   transfer in vertebrates. *Nat Genet* 2009; **41**: 753–761.

917 79 Waldo GS, Standish BM, Berendzen J, Terwilliger TC. Rapid protein-folding assay using

918   green fluorescent protein. *Nat Biotechnol* 1999; **17**: 691–5.

919 80 Kozak M. An analysis of 5'-noncoding sequences from 699 vertebrate messenger RNAs.

920   *Nucleic Acids Res* 1987; **15(20)**: 8125–8148.

921 81 Gasteiger E, Hoogland C, Gattiker A, Duvaud S, Wilkins MR, Appel RD *et al.* Protein

922   identification and analysis tools in the ExPASy server. In: Walker JM (ed). *The*

923   *Proteomics Protocols Handbook*. Humana Press, 2005, pp 571–607.

924 82 Robinson M, McCarthy D, Smyth G. edgeR: a Bioconductor package for differential

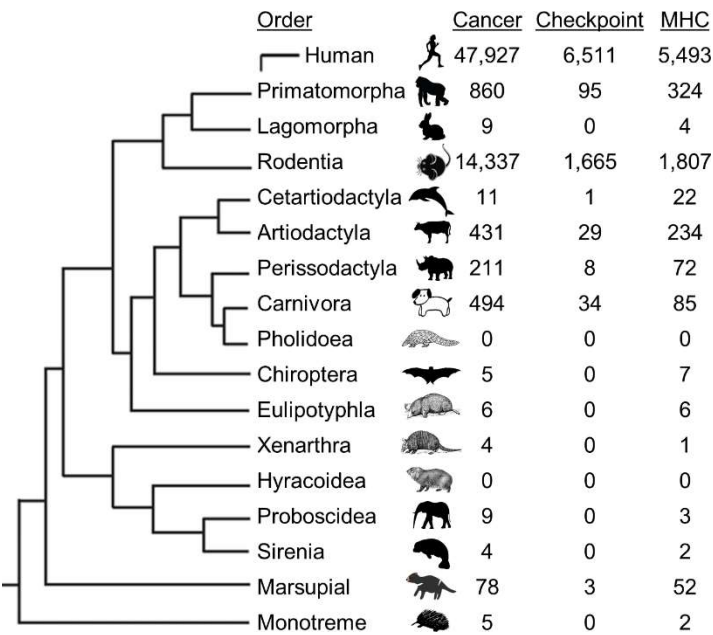925   expression analysis of digital gene expression data. *Bioinformatics* 2010; **26**: 139–140.

926

927

928

929

930 **FIGURES**

931

Order		Cancer	Checkpoint	MHC
Human		47,927	6,511	5,493
Primatomorpha		860	95	324
Lagomorpha		9	0	4
Rodentia		14,337	1,665	1,807
Cetartiodactyla		11	1	22
Artiodactyla		431	29	234
Perissodactyla		211	8	72
Carnivora		494	34	85
Pholidoea		0	0	0
Chiroptera		5	0	7
Eulipotyphla		6	0	6
Xenarthra		4	0	1
Hyracoidea		0	0	0
Proboscidea		9	0	3
Sirenia		4	0	2
Marsupial		78	3	52
Monotreme		5	0	2

932

933

934 **Figure 1. Phylogenetic tree of immune system related studies in mammal orders 2009-2019.**

935 Metastatic cancer has been reported in nearly all mammalian orders and major histocompatibility

936 complexes (MHC) have been the most intensely studied molecules in most orders. In the past

937 decade, studies of immune checkpoint molecules (PD1, PDL1, CTLA4) have become a primary

938 focus in humans and rodents. However, immune checkpoint studies in other species are limited,

939 particularly at the protein level, due to the lack of species-specific reagents. This creates a vast gap

940 in our understanding of the evolution of the mammalian immune system. The numbers in the

941 columns represent the number studies matching Web of Science search results between 2009-2019.

942 See Table S1 for search terms.
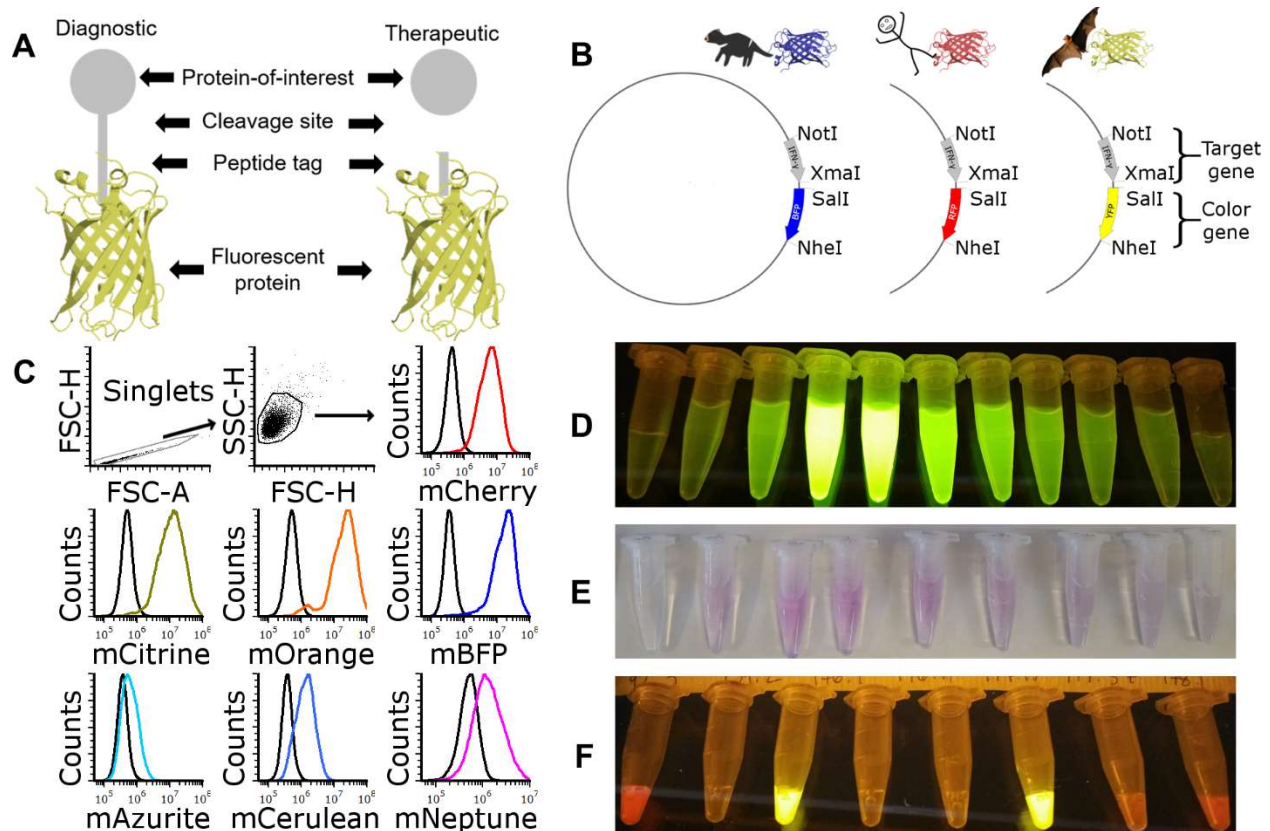
Figure 2. FAST protein schematic and initial testing. (A) Schematic diagram of FAST protein therapeutic and diagnostic (i.e. theranostic) features and (B) vector map showing restriction sites for swapping the target gene (i.e. gene-of-interest) and color genes (i.e. fluorescent protein). (C) Results of flow cytometry binding assay with devil 41BB FAST proteins. The colored lines in the histograms show binding of devil 41BB fused to mCherry, mCitrine, mOrange, mTagBFP, mAzurite, mCerulean3, or mNeptune2 to CHO cells transfected with devil 41BBL, and the black lines show binding to untransfected CHO cells. (D-E) Images showing the gradient of FAST proteins eluted from HisTrap columns. (D) mCitrine excited with blue light and (E) chromogenic visualization of mCherry without excitation. (F) Image of 100 μL of FAST protein excited with blue light (NOTE: mBFP appears clear with blue excitation and amber filter unit).

955
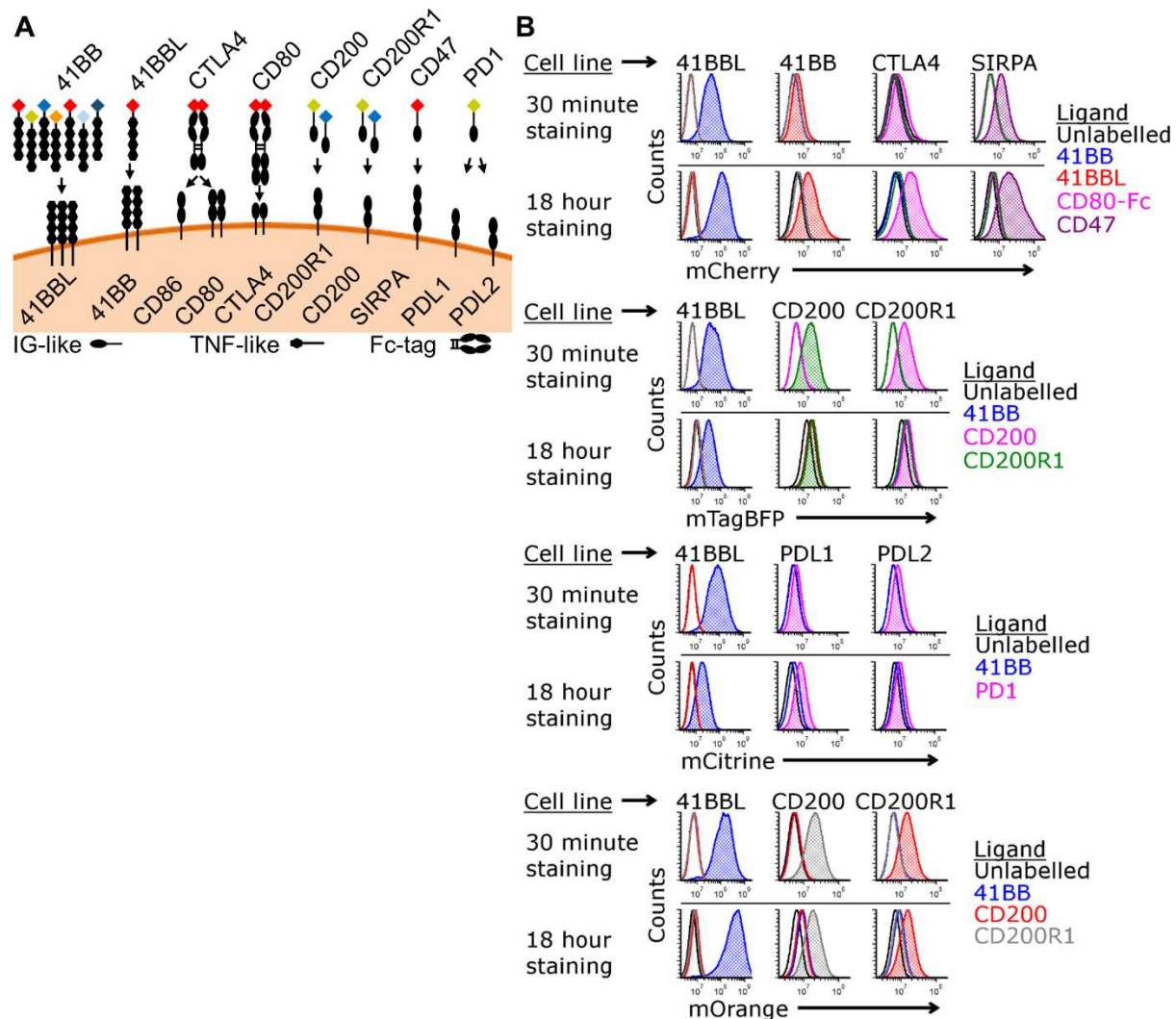
Figure 3. Map and testing of soluble proteins FAST proteins. (A) Diagram of soluble FAST proteins and full-length proteins used for testing of FAST proteins. 41BBL is a type II transmembrane protein; all other proteins are type I. CD80 and CTLA4 soluble FAST proteins included a devil IgG Fc-tag. Arrows indicate interactions confirmed in this study. (B) Histograms showing binding of FAST proteins to CHO cells expressing full-length devil proteins. Target CHO cells were cultured with chloroquine to block lysosomal degradation of FAST proteins and maintain fluorescent signal during live-culture binding assays with 2 μg/well of purified FAST proteins for 30 minutes or 18 hours to assess receptor-ligand binding (n=1/time point).

964
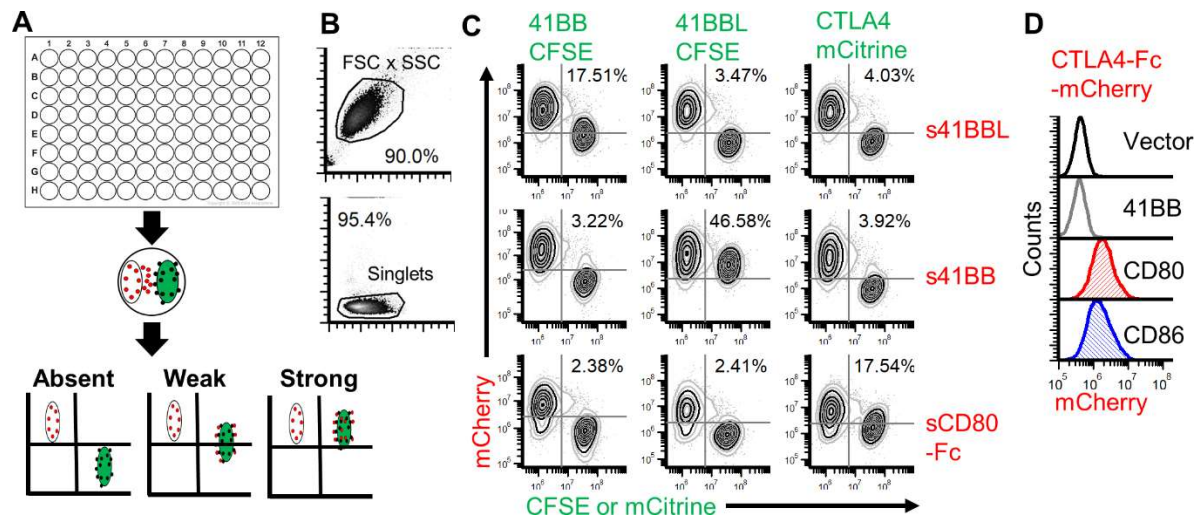
Figure 4. Live-cell coculture assays with FAST proteins. (A) Schematic of coculture assays to assess checkpoint molecule interactions (Absent, Weak, Strong). Cells were mixed and cultured overnight with chloroquine. Protein binding and/or transfer were assessed using flow cytometry. (B) Gating strategy for coculture assays. (C) CHO cells that secrete 41BBL-mCherry, 41BB-mCherry, or CD80-Fc-mCherry were cocultured overnight with target CHO cells that express full-length 41BB, 41BBL, or CTLA4. 41BB and 41BB-L were labeled with CFSE, whereas full-length CTLA4 was directly fused to mCitrine. Cells that secrete mCherry FAST proteins appear in the upper left quadrant. Cells expressing full-length proteins and labeled with CFSE or mCitrine appear in the lower right quadrant. Cells in the upper right quadrant represent binding of mCherry FAST proteins to full-length proteins on CFSE or mCitrine labeled cells. Results shown are representative of n=3/treatment. (D) CTLA4-Fc-mCherry FAST protein binding to DFT cells. DFT1 C5065 cells transfected with control vector (black), 41BB (gray), CD80 (red), or CD86 (blue) were stained with CTLA4-Fc-mCherry supernatant with chloroquine. Results are representative of n=2 replicates/treatment.

47

981
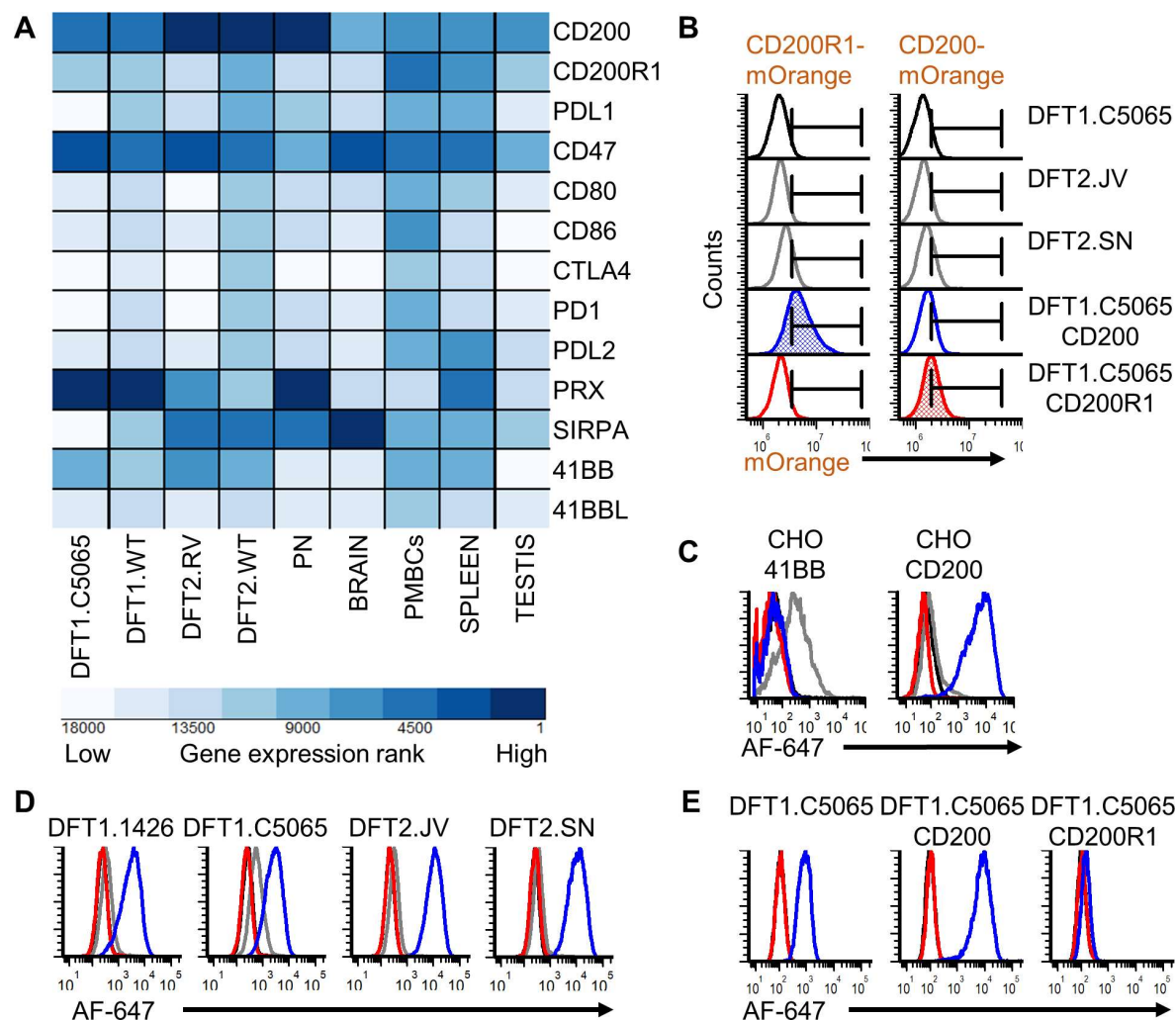
Figure 5. Elevated CD200 expression on DFT cells. (A) Heatmap showing within sample

transcript ranking (1 = highest expression) according to RPKM-normalized mRNA sequencing

counts of 18,788 annotated coding genes (devil_refv7.0; GCA_000189315.1). Genes-of-interest

for this study are plotted as heatmap with dark blue indicating the most highly expressed genes.

Technical replicates (n=2) were used for all tissues, except peripheral nerve (PN) (n=1). (B) Wild

type DFT1.C5065, DFT2.JV, DFT2.SN, and DFT1.C5065 transfected to overexpress CD200 or

CD200R1 were stained with 5 μg of either CD200R1-mOrange or CD200-mOrange FAST protein.

Histograms filled with blue or red highlight the cells overexpressing CD200 or CD200R1 and their

expected binding interactions with CD200R1 and CD200, respectively. Target cells were cultured

48

991   with FAST proteins in chloroquine, incubated 30 minutes, and run without washing. Results are

992   representative of n=2 replicates/treatment. (C) Mice were immunized with TEV digested 41BB or

993   CD200 FAST proteins. Black = pre-immune (PI) and gray = immune (I) sera from a mouse

994   immunized with 41BB; red = pre-immune (PI) and blue = immune (I) sera from a mouse

995   immunized with CD200. CHO cells transfected with either full-length 41BB or CD200 were

996   stained with sera and then anti-mouse AlexaFluor-647. Results are representative of

997   n=2/treatment. (D) Sera was used to screen two strains of DFT1 and two strains of DFT2 cells for

998   41BB and CD200 expression. PI sera was negative in all cases, whereas all DFT1 and DFT2 cells

999   expressed CD200. Results are representative of n=3/treatment. (E) DFT1 C5065 transfected with

1000   either vector control, CD200, or CD200R1 were stained with purified polyclonal anti-CD200 and

1001   anti-mouse IgG AlexaFluor 647 (black = no antibodies, red = secondary antibody only, blue =

1002   primary + secondary antibody). Results are representative of n=2/treatment.

1003

1004

1005
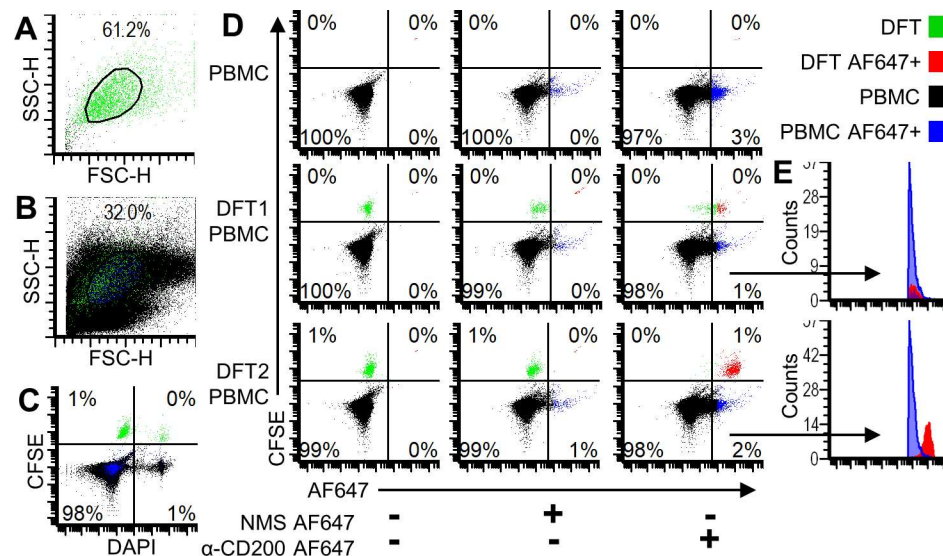
1006 **Figure 6. CD200 identifies DFT cells in whole blood.** Color dot plots showing DFT cells in green

1007 (CFSE), PBMCs in black, DFT Alexa Fluor 647+ (AF647) cells in red, and PBMC AF647+ in

1008 blue. (A) Forward- and side-scatter plot of DFT.JV cells and (B) DFT.JV cells mixed with PBMCs.

1009 (C) Color dot plot showing dead cells stained with DAPI (right quadrants) and CFSE-labeled DFT

1010 cells (upper quadrants). (D) The top row shows unmixed PBMCs. The middle row and bottom row

1011 show DFT1.C5065 and DFT2.JV cells, respectively, mixed with PBMCs. Alexa Fluor 647+ DFT

1012 (red) and PBMC (blue) are in the right quadrants. (E) Histogram overlays to highlight AF647+

1013 (right quadrants) from DFT1-PBMC and DFT2-PBMC mixtures. Cells were analyzed on the

1014 Beckman-Coulter MoFlo Astrios.

1015

1016 **TABLES (See supplementary Materials)**

1017

1018

1019

1020

50

SUPPLEMENTARY INFORMATION

TITLE

A novel system to map protein interactions reveals evolutionarily conserved immune evasion pathways on transmissible cancers

SHORT TITLE

Immune checkpoints on transmissible cancers

AUTHORS

Andrew S. Flies[1]*, Jocelyn M. Darby[1], Patrick R. Lennard[1,2], Peter R. Murphy[1,3], Chrissie E. B. Ong[1], Terry L. Pinfold[4], A. Bruce Lyons[4], Gregory M. Woods[1], Amanda L. Patchett[1]

AFFILIATIONS

[1]Menzies Institute for Medical Research, College of Health and Medicine, University of Tasmania, Hobart, TAS 7000, Australia

[2]The Roslin Institute and Royal School of Veterinary Studies, University of Edinburgh, Easter Bush Campus, Midlothian, EH25 9RG, UK

[3]University of Queensland Diamantina Institute, The University of Queensland, Translational Research Institute, Woolloongabba, Queensland, Australia

[4]School of Medicine, College of Health and Medicine, University of Tasmania, Hobart, TAS 7000, Australia

51

CORRESPONDING AUTHOR CONTACT INFORMATION

Andrew S. Flies, PhD

Menzies Institute for Medical Research

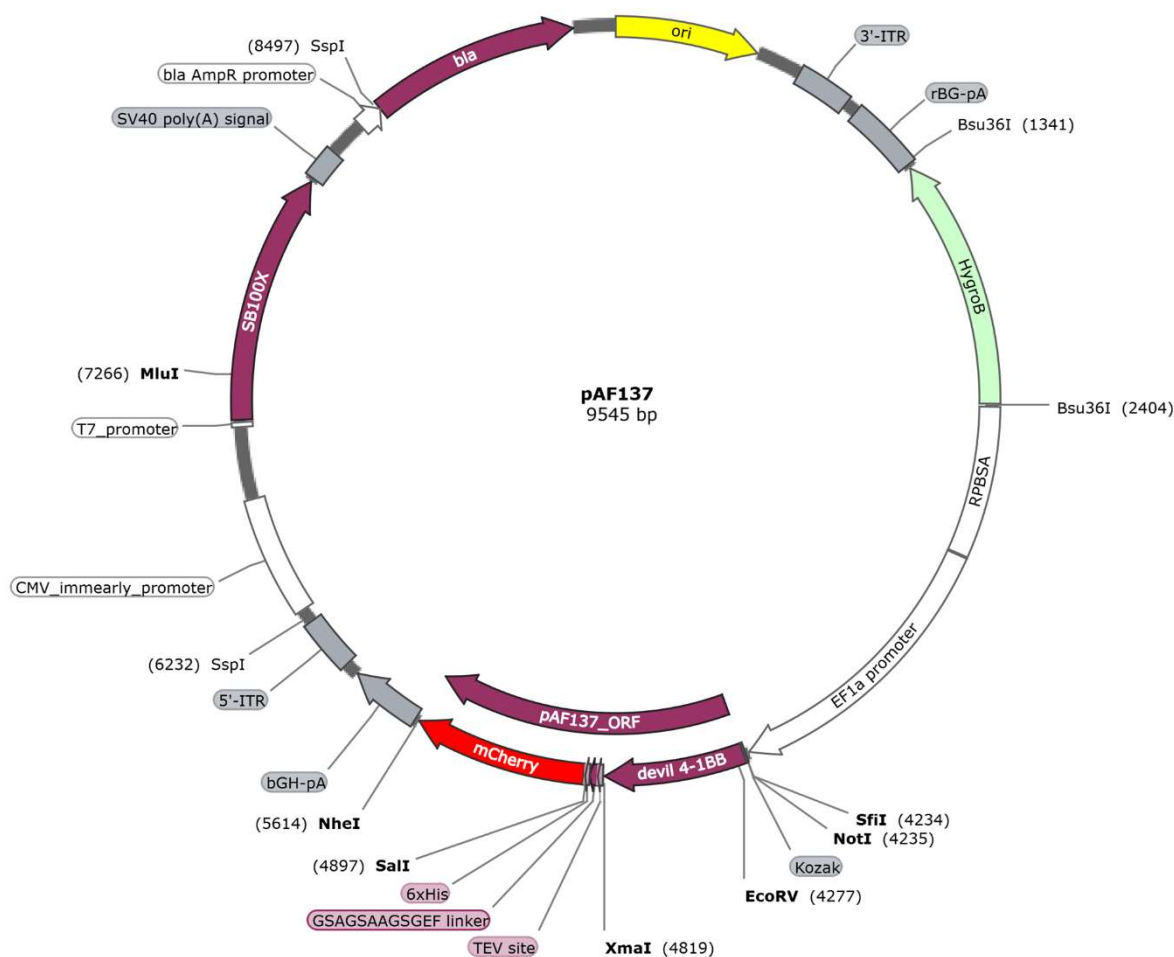College of Health and Medicine

University of Tasmania
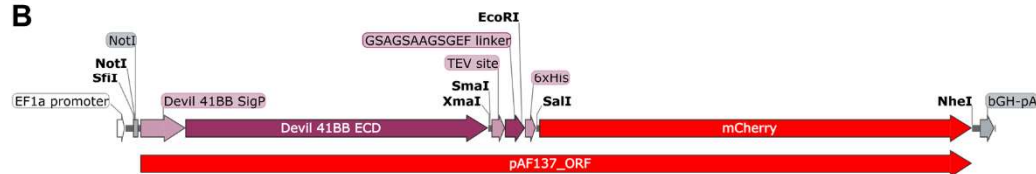
Private Bag 23, Hobart TAS 7000

phone: +61 3 6226 4614

email: Andy.Flies@utas.edu.au
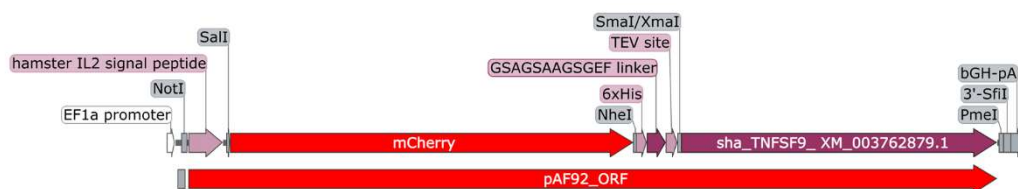
1054   **SUPPLEMENTARY MATERIALS AND METHODS**

1055

54

1056   **Figure S1. FAST protein base vectors.** (A) CMV promotor and SB100X transposase were

1057   inserted into a Sleeping Beauty vector (shown here with 41BB-mCherry FAST protein cassette

1058   pAF137). (B) Type I FAST protein cassette. The native signal peptide (SigP) and predicted

1059   extracellular domain (ECD) were used for all type I FAST proteins. The devil 41BB SigP-ECD

1060   was fused to mCherry via a TEV cleavage site (ENLYFQG), linker peptide (GSAGSAAGSGEF),

1061   and a 6x-His tag (HHHHHH). Restriction digest sites were included at the 5' and 3' ends of the

1062   gene-of-interest and the fluorescent protein to facilitate swapping of genes and fluorescent

1063   proteins. The human EF1α promotor is upstream and bovine growth hormone (bGH) poly(A) tail

1064   is downstream of the open reading frame. (C) Type I FAST protein cassette with Fc tag. This

1065   vector was the same as the type I FAST vectors, except that the Fc fragment of devil IgG was

1066   inserted between the gene-of-interest (e.g. CD80) and the TEV cleavage site. (D) Type II FAST

1067   protein cassette. To increase the probability of efficient secretion of type II FAST proteins from

1068   Chinese hamster ovary (CHO) cells, we used the hamster IL-2 signal peptide at the N-terminus of

1069   the protein, including a SalI restriction site, followed by mCherry, an NheI restriction site, 6x-His-

1070   tag, linker peptide, TEV cleavage site, XmaI/SmaI restriction site, the gene-of-interest, and a PmeI

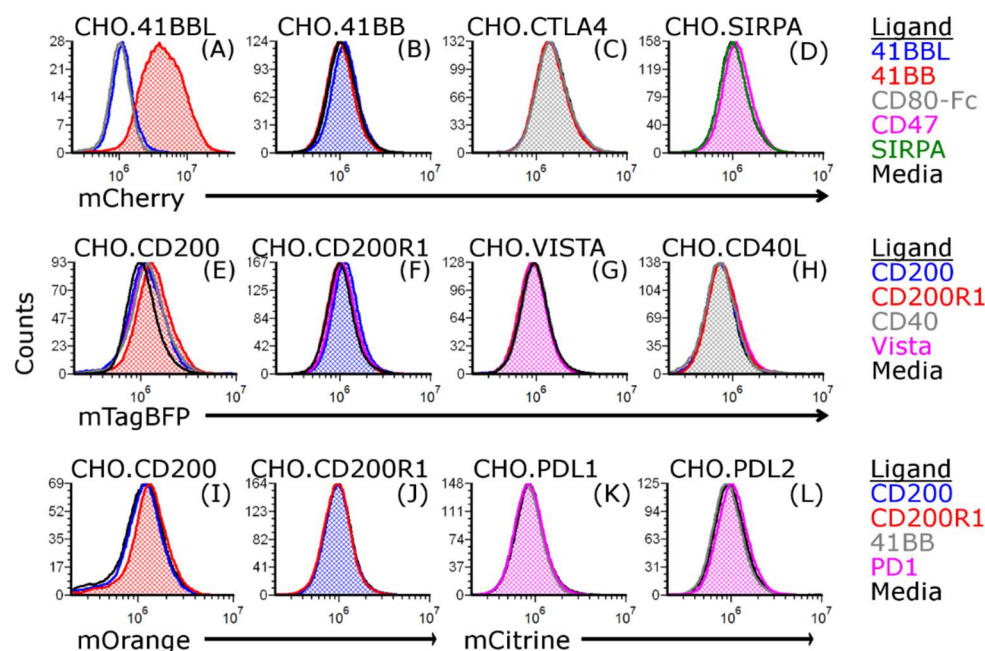1071   restriction site following the stop codon.

1072

1073

Figure S2. Screening FAST protein supernatants. Staining was performed using supernatants from FAST protein CHO cell lines; supernatants were collected 11 days post-transfection. Supernatants from FAST cell lines were incubated with CHO cells expressing full-length devil proteins at room temperature for 30 minutes before washing and fixing for flow cytometric analysis. Chloroquine was not used during these incubation steps.
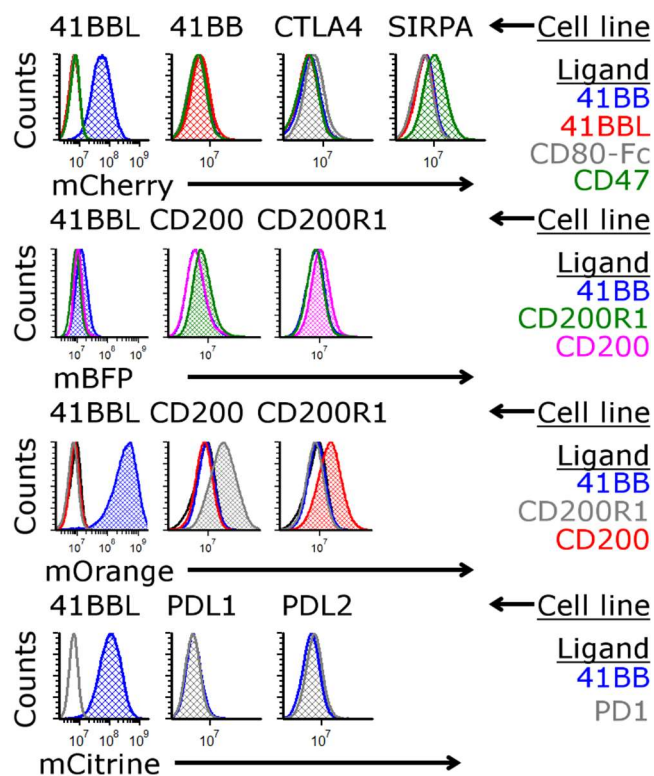
1079

1080

Figure S3. Screening FAST protein supernatants. Staining was performed using supernatants from FAST protein CHO cell lines; supernatants were collected around 2-3 weeks post-transfection and stored for 2 months at 4 °C. Supernatants from FAST cell lines were diluted 1:1 with 100 µM chloroquine (50 µM final concentration) in cRF5 without phenol red incubated with CHO cells expressing full-length devil proteins at room temperature for 60 minutes before washing and fixing for flow cytometric analysis.
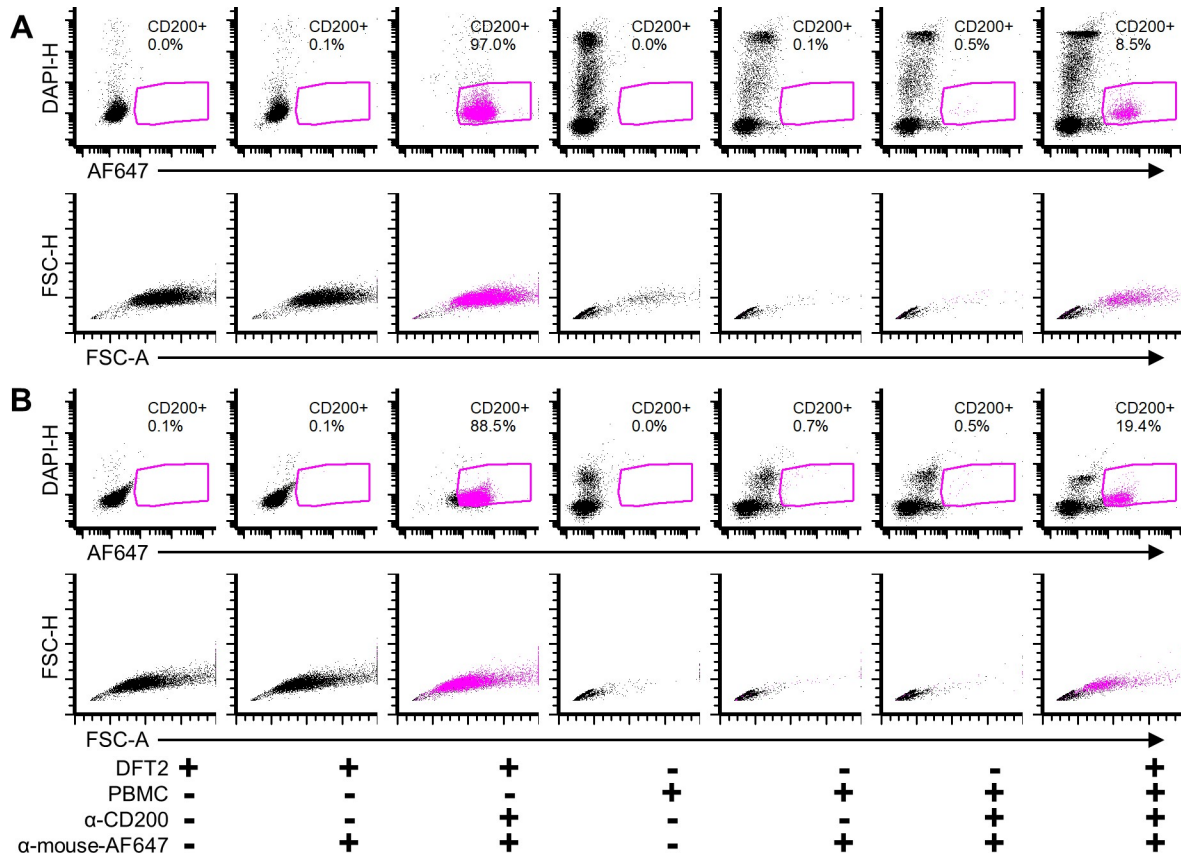
1081

1082

1083

1084

1085

1086

1087

1088

1089

57

1090

Figure S4. CD200 identifies DFT2 cells in PBMCs. (A) PBMCs isolated on histopaque, frozen, thawed, and cultured for 2 hours at 37 °C prior to use. DFT2 cells and PBMCs were stained separately by blocking with normal goat serum and then staining with anti-CD200 serum and anti-mouse IgG Alexa-647. Cells were then washed, stained with DAPI, and analyzed on a BD FACSCanto II. The stained DFT2 cells and PBMCs were then mixed at 1:10 to see if gating and CD200 signal could be used to distinguish DFT2 cells from PBMCs (n=1/treatment). (B) The procedure used for A was repeated except that DFT2 cells and PBMCs were mixed at 1:5.
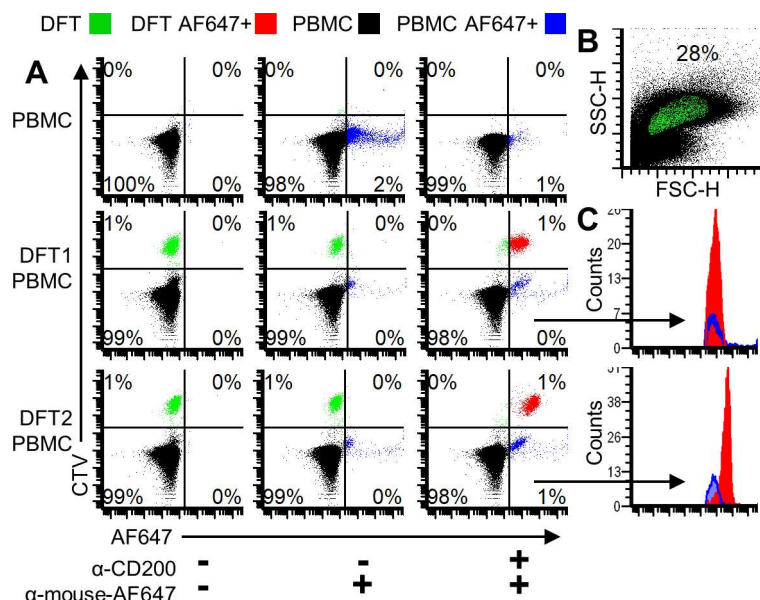
Figure S5. CD200 identifies DFT cells in whole blood. Color dot plots showing DFT cells in green (CellTrace Violet®), PBMCs in black, DFT Alexa Fluor 647+ (AF647) cells in red, and PBMC AF647+ in blue. (A) The top row shows unmixed PBMCs. The middle row and bottom row show DFT1.C5065 and DFT2.JV cells, respectively, mixed with PBMCs. Alexa Fluor 647+ DFT (red) and PBMC (blue) are in the right quadrants. (B) Forward- and side-scatter plot of DFT.JV cells mixed with PBMCs. Backgating of CFSE+ cells was used to create a forward-scatter by side-scatter gate thaat was used as the parent gate for all data shown here. (C) Histogram overlays to highlight AF647+ (right quadrants) from DFT1-PBMC and DFT2-PBMC mixtures. Cells were analyzed on the Beckman-Coulter MoFlo Astrios.

1091

1092

1093

1094

1095 **Table S1. Search terms for mammalian immune research studies.**

1096

1097 **Table S2. Summary and genes and plasmids.**

1098

1099 **Table S3. Vector backbones and insert cassette components.**

1100

1101 **Table S4. Primer sequences and gBlocks for plasmid assembly.**

1102

1103 **Table S5. gBlocks used for assembling plasmids.**

1104

1105